SIMULATION OF DIFFERENT BUBBLE DYNAMICS MODEL AND DEVELOPMENT OF OPTICAL TECHNIQUE FOR DETECTION OF BUBBLE

A Dissertation Submitted

To

Sikkim University

In Partial Fulfilment of Requirement for the
Degree of Master of Philosophy

By

VIVEKANANDA MAHATO

Department of Physics
Schoool of Physical Science

February, 2018.

Abstract

Cavitation in liquid medium and its dynamics has been modeled by a number of researchers. Assuming compressibility and incompressibility a number of models like Rayleigh-Plesset's model, Gilmore's model, Flynn's model, Herring's model, Keller-Miksis's model etc were proposed. The qualitative and quantitative differences between these models had been tested in experimental study of cavitation bubble dynamics as well as by simulation work. On the other hand bubble detection by optical technique is an effective as well as superior method.

In the theoretical part of our thesis we have chosen five well-known models namely, (1)Rayleigh-Plesset's model, (2)Gilmore's model, (3)Flynn's model, (4)Herring's model, (5)Keller-Miksis's, that effectively describes the dynamics of a bubble in an incompressible and compressible liquid media respectively. Our simulation was performed on bubbles filled with both ideal gas as well as Van der Waals type gas. The objective of our work was to investigate the qualitative and quantitative differences, that are evident in the bubble dynamics, as predicted by these different models. We also attempted for a parameter optimization, in case of some models, that would be relevant for any experimental investigation on bubble dynamics.

In optical detection technique of bubble we have used a single photodiode to study the beam deflection due to the interaction of probe laser beam with air bubble. The beam deflection phenomena studied for different probe beam diameter, medium in which air bubble resides .

Dedication

To my family...

Acknowledgements

It is a good experience working under the guidance and supervision of Dr. Ajay Tripathi and Dr. Souvik Chatterjee. I wish to express my deep sense of gratitude and respect to Dr. Ajay Tripathi for providing me an opportunity to work in his laboratory as well as Dr. Souvik Chatterjee to guide in simulation work. Also I would like to thank both of them for their encouragement throughout the preparation of my M.Phil. dissertation work. Under their guidance I feel interested to work in experimental as well as theoretical field of Cavitation Bubble Dynamics.

The faculty members, Dr. Subir Mukhopadhyay, Dr. Hemam Dinesh Singh, Dr. Archana Tiwari, Dr. Amitabha Bhattacharyya, have always welcomed and encouraged me since the very first day, so my heartfelt gratitude to them.

I would also like to express thank to Mr. Indra Hang Subba, Mr. Rajesh Rawat, Mr. Nishal Rai, Mrs. Ambika Pradhan, Miss Trisha Mondal for their serious assistance during my work. I would also like to thank all my friends, seniors in and out of Sikkim University for their care and kind support.

Last but not the least; I pay my special gratitude to my family members for their ceaseless love and perpetual encouragement. Many others remain unthanked by name. A heartfelt word of gratitude to all those who touched my life during these years.

Contents

List of Figures

Chapter 1

Introduction

1.1 Introduction

Cavitation in liquid medium and the dynamics of cavitation bubble has been a great interest of research since the early twentieth century. Due to the recent applications in Medical Science, Envioronmental Science, Technology it is necessery to study the dynamics of cavitation bubble in liquid medium, cavitation bubble generation techniques, cavitation bubble detection techniques etc.

Lord Rayleigh first studied the spherical bubble collapse to explain the damage of propellers of high speed boats and submarines in 1917 [1]. He made the assumption that the liquid was incompressible and the cavity was empty. Furthermore, he neglected liquid viscosity, surface tension, evaporation, condensation, gas diffusion, heat conduction, and instability (which leads to aspherical flow). Still, his results agreed fairly well with experiment over a large portion of the bubble motion.

Modifications and extensions of Rayleigh's work have been made by a number of researchers. Herring [2] and Trilling [3], used the quasi-acoustic approximation (liquid velocities are small compared to the velocity of sound) to provide a first-order correction for the compressibility of the liquid considering surface tension, viscosity and other properties of the liquid.

Higher order compressibility effects were treated by Gilmore [4] whose model of cavitation bubble dynamics, which was based on the Kirkwood-Bethe hypothesis [5], also includes viscosity, surface tension, and a constant gas content in the bubble.

Flynn proposed a model very similar to Rayleigh-Plesset model but it takes into account the compressibility in the far field and in-

compressility in near field [6]. His model describes the dynamical motions of small cavitation bubbles in liquids set into motion by an acoustic pressure field. The mathematical formulation takes into account heat conduction inside a bubble and in the surrounding liquid, and the effect of viscosity, compressibility, and surface tension of the liquid also taken into account.

Keller and Miksis derived a cavitation bubble dynamics model for large amplitude forced oscillation in a sound field [7]. Here they have considered compressibility of the liquid, constant velocity of sound in the liquid .

In addition to these early studies, other reports have sought to make refinements and corrections to account for other conditions present during the collapse. For example, Fujikawa and Akamatsu [8] have studied the bubble dynamics, accounting for condensation, heat conduction, and temperature discontinuity at the phase interface.

In late 90's some researchers have proposed bubble models for Ultrasound Contrast Agent(UCA) encapsulating bubble. For example, De Jong [9] and his group did some experimental studies in ultrasound contrast agent and modeling by their theoretical description of the vibration of an encapsulated microbubble. This model was about gas bubble in water and the bubble coated by albumin. This model is based on Rayleigh-Plesset equation. Church [9] derives his UCA bubble model from Rayleigh-Plesset model that accounted for the shell thickness and visco-elastic properties. Hoff et. al.[10] derives his model from Church in the limit of small shell thickness in comparison with the radius. Morgan [9] constructed his model from Herring equation [2]. Coating effects are represented by two additional terms. The first term incorporates the elasticity of the shell. The second term is a damping term because of the viscosity of the shell and is similar to the terms derived by Church. Chatterjee-Sarkar [9] considered viscous interfacial stresses in their model. The model considers thin-shelled agents. Marmottant [11] took into account the physical properties of a lipid monolayer coating on a gas microbubble in his model. Three parameters describe the properties of the shell: a buckling radius, the compressibility of the shell, and a break-up shell tension. The model presents an original non-linear behavior at large amplitude oscillations, termed compression-only, induced by the buckling of the lipid monolayer.

Due to Micro and Nano Bubble's application in Medical Science

as drug delivery agent, Ultrasonography contrast agent etc., it is necessery to detect them as precise as possible. Detection of cavitation bubble may be done by, which occurs on a microsecond time scale, using a high speed photography [12, 13, 14], optical probe techniques [15, 12], using a photodiode [16], using high speed photography with a CCD camera [12, 14, 13], Schlieren photography [17, 18], Interferometry [19], Shadow photography [13, 20] ultrasound transducer [12] etc.

1.2 Structure of the Thesis:

In **Second Chapter**, literature review of different bubble dynamics model and detection techniques of cavitation bubble has been done.

In **Third Chapter**, at first, basic cavitation theory is discussed and then different cavitation bubble dynamics model were introduced.

In **Fouth Chapter**, simulation results on bubble dynamics have been discussed. At first with the help of simulation results a comparative study between different models have been done. Then parameter optimization of a particular model was done by simulation work.

In **Fifth Chapter**, developed optical detection technique for cavitation bubble has been discussed. Later the probe beam deflection result has given.

In **Sixth** and the final chapter, conclusion and future prospects of our work has been discussed.

Chapter 2

Review of Literature

This section is devided into three part. In first part a thorough literature review for cavitation bubble dynamics models has been done. In second part the bubble formation and the factors effecting bubble formation in a liquid column has been discussed. In third and final part detection techniques, used mostly, for cavitation bubble are reported.

2.1 Review of Bubble Dynamics Models:

Lord Rayleigh first studied the spherical bubble collapse to explain the damage of propellers of high speed boats and submarines in 1917 [1]. He made the assumption that the liquid is incompressible and the spherical cavity in the liquid is empty. He has neglected liquid viscosity, surface tension, evaporation, condensation, gas diffusion, heat conduction and other instability factors. Still, instead of all this approximation, his results agreed well with experiment over a large portion of the bubble motion.

Later some significant modifications and extensions of Rayleigh's work have been made by a number of researchers. For example, Herring [2] and Trilling [3], used the quasi-acoustic approximation i.e. liquid velocities are small compared to the velocity of sound and gave bubble dynamics equation with first-order correction of the compressibility of the liquid considering surface tension, viscosity and other properties of the liquid.

Higher order compressibility effects were included by Gilmore [4] in his cavitation bubble dynamics model, which is based on the Kirkwood-Bethe hypothesis [5], also includes viscosity, surface tension, and a constant gas content in the cavity bubble.

Flynn proposed a model very similar to Rayleigh-Plesset's model

but it takes into account the compressibility in the far field and incompressility in near field [6]. His model describes the dynamical motions of small cavitation bubbles in liquids which are set into motion by an external acoustic pressure field. Flynn in development of mathematical formulation for cavitation bubble dynamics considered heat conduction inside a bubble and in the surrounding liquid, and the effect of viscosity, compressibility, and surface tension of the liquid has also taken into account.

Keller and Miksis derived a cavitation bubble dynamics model for large amplitude forced oscillation in a sound field [7]. Here they have considered compressibility of the liquid, constant velocity of sound in the liquid and a first order acoustic approximation .

In addition to these early studies, other reports regarding the refinements and corrections for conditions present during the collapse of a bubble has also been made. For example, Fujikawa and Akamatsu [8] have studied the bubble dynamics, accounting for condensation, heat conduction, and temperature discontinuity by considering a non-equlibrium interface of the bubble.

In late 90's some researchers have proposed bubble models for Ultrasound Contrast Agent(UCA) encapsulating bubble. For example, De Jong [9] and his group did some experimental studies on ultrasound contrast agent and it's modeling by their theoretical description of the vibration of an encapsulated microbubble. This model was about gas bubble in water and the bubble coated by albumin. It is based on Rayleigh-Plesset's bubble dynamics equation. Church [9] derives his UCA bubble model from Rayleigh-Plesset's model by considering shell thickness and a viscoelastic properties of bubble interface. Hoff et al. [10] derived his model from Church in the limit of small shell thickness of bubble in comparison with the radius. Chatterjee-Sarkar [9] proposed a UCA bubble model considering thin-shelled agents at the interface.

2.2 Air Bubble In a Liquid Column:

When any object rises or falls through a fluid it will experience a viscous drag, whether it is a parachutist or spacecraft falling through air, a stone falling through water or a bubble rising through a liquid column. This type of problem was formulated by Stokes and is therefore known as Stokes' law. Let us consider a spherical body of radius r,

mass m, density ρ falling through a fluid(see figure 2.1) of viscosity μ, density ρ due to gravitational acceleration g with a velocity v. So, it will experience a viscous drag due to viscosity.

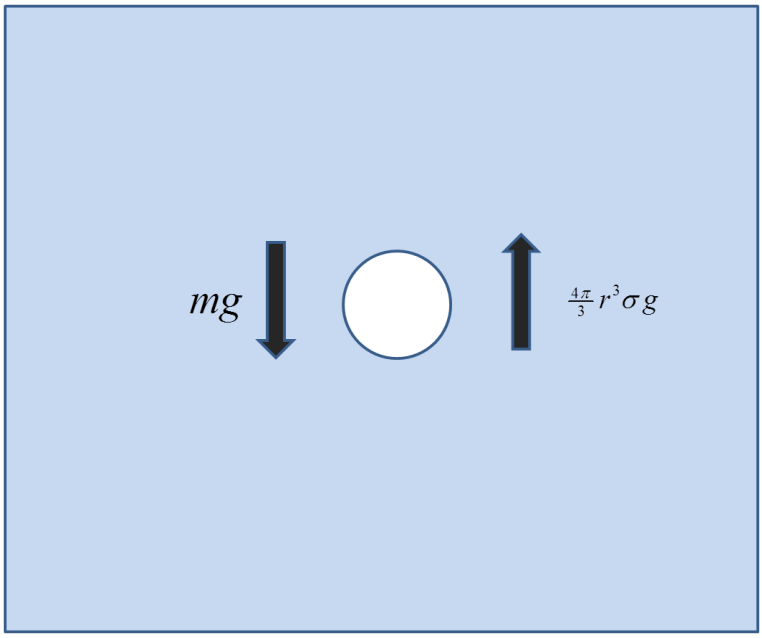

Figure 2.1: A spherical body falling through a viscous liquid. Effective force on it is due to the resultant of gravitational force and upthrust.

Acording to Stoke's Law, effective gravitational force = weight - upthrust = $4/3\pi r^3 g(\rho - \sigma)$

As the body falls so its velocity increases until it reaches a constant velocity known as the terminal velocity. At the terminal velocity the frictional drag due to viscous forces is just balanced by the gravitational force and hence the velocity is constant as shown by Figure 2.2.

At terminal velocity, effective gravitational force = viscous drag

$$6\pi r v \eta = 4/3\pi r^3(\rho - \sigma)g \tag{2.1}$$

or,

$$v = \frac{2}{9}\frac{gr^2(\rho - \sigma)}{\mu} \tag{2.2}$$

Stokes's law shows that the viscous drag (F) is directly proportional to the weight of the sphere, in other words F is proportional to r^3. The formula for velocity shows that the terminal velocity (v) is proportional to the square of radius; v is greater for a larger sphere than for a smaller one of the same material.

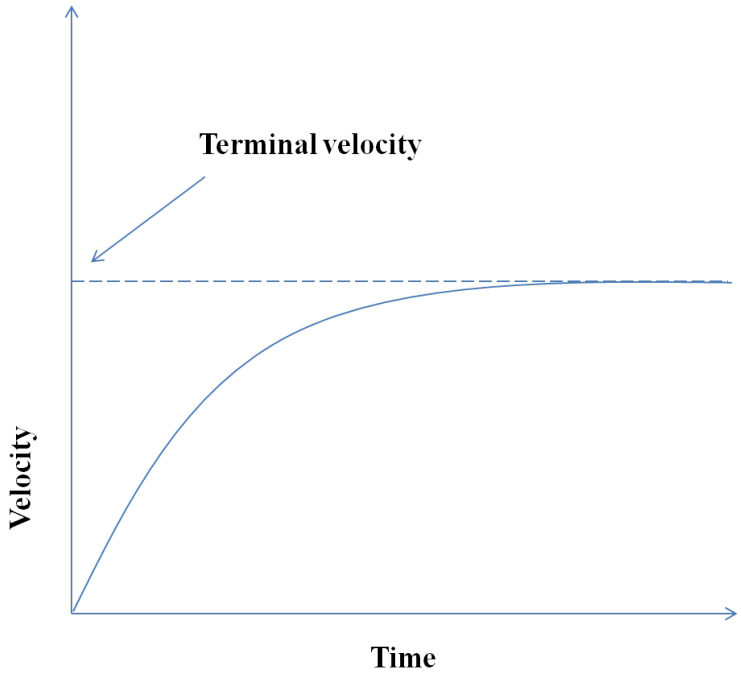

Figure 2.2: Velocity of an object will increase with time as it falls through a viscous fluid and after some time attains a contant velocity i.e. terminal velocity.

In equation (2.2) if $(\rho - \sigma) > 0$ then v is positive i.e. the body will move downwards due to gravity. This can be seen for any massive object when it falls from a height due to gravity. If $(\rho - \sigma) < 0$ then v is negative i.e. the body will move upwards. This happens when a bubble is formed in a liquid medium.

2.3 Factors of Bubble Formation Through an Orifice in Liquid:

The process of bubble formation is governed by a number of parameters like gas flow rate through the orifice, orifice geometry, liquid chamber volume, viscosity, density, ploarity of the liquid effects bubble formation and also decides the bubble size [21].

Viscosity of Liquid: Due to the change in viscosity of the liquid, the magnitude of viscous forces exerted during bubble formation changes such that a stable bubble diameter is attainedby the bubble before its detachment from tne orifice. Most interesting fact is that the experimental observations by various investigators are contradicting one another. For example (1) Khurana et al.[22] reported that bubble size increases with liquid viscosity, (2) Benzing et al.[23], Kumar et al.[24]

reported that bubble size are independent of liquid viscosity and (3) Vasilev et al. [25] said that viscosity has very small effect on bubble size so that it can be neglected.

Surface Tension of Liquid: There are two types of surface tension forces act on a bubble. They are dynamic and static. During the initial part of bubble's growth phase, the surface tension is dynamic because of the contact angle of the bubble with the orifice changes continuously and during the final stage of growth the contact angle reaches a constant value. This implies a static surface tension. So surface tension decides the time of growth of bubbles[21]. In a work Kulkarni [21] reported that for small diameter orifices, the effect of surface tension is negligible if the gas flow rate is high and for constant gas flow rate, the surface tension loses its dominance.

Density of Liquid: Khurana et. al.[22] reported that (1)for small flow rate and viscosity there is a decrease in bubble volume with the increase in liquid density. (2) If the flow rate is large and viscosity is small then the bubble volume is independent of liquid density for small orifice diameter. And, also for both small orifice diameter and viscosity, again the second statement is turns out to be true.

Orifice Diameter: Bubble formation in a liquid can be realise by injecting a gas through a orifice, diapharm or puncture in a membrane. The improtant orifice related parameter in bubble formation are type of orifice, orifice chamber volume, orifice submergence etc. Tsuge et.al. [26] observed that the diameter effect in small orifices is negligible, while for large diameter orifices, the bubble volume increases with flow rate.

2.4 Bubble Rise Velocity in Liquid Column

The single isolated air or gas bubble's rising velocity in a liquid depends on buoyancy and drag forces. Bubble shape and motion in liquid goes effected by surface tension, viscosity, inertia and buoyancy. Rise velosity (u) of perfectly spherical, small, isolated, bubble is given by Stokes solution as

$$u = \frac{1}{18}\frac{gr^2(\rho_l - \rho_g)}{\mu} \tag{2.3}$$

Where g= acceleration due to gravity. r= bubble diameter. ρ_l= density of the liquid. ρ_g= density of the gas inside the bubble. μ= dynamic vescosity of the liquid. This relation holds true for small sized bubble because of the dominant effect of surface tension on the shape of small sized bubble.

When isolated bubbles are very large, surface tension effects and viscosity are neglegible and rise velocity is given by Davies and Taylor [27] as

$$u = 0.707\sqrt{gr} \tag{2.4}$$

For intermediate size bubbles, effects of liquid inertia, surface tension, viscosity and cleanliness as well as whether bubbles rise in straight lines, oscillate, or describe a spiral path are important.

2.5 Review of Bubble Detection Techniques:

Due to Micro and Nano Bubble's application in Medical Science as drug delivery agent, Ultrasonography contrast agent and also in the field of technology, it is necessery to detect cavitation bubble as precise as possible. Detection of cavitation bubble may be done by, which occurs on a microsecond time scale, optical probe techniques [15], using a photodiode [16], using high speed photography [12, 14, 13], Schlieren photography [17, 18], Interferometry [19], Shadow photography [13, 20] and pizo-electric ultrasound transduser [28] etc.

2.5.1 Shadow Photography:

In shadow photography [13, 20] generally a pump beam is used to generate optical breakdown in some liquid medium. The probe beam is expanded rather than focused and used as illuminating light (perpendicular to the pump beam) to image the focal volume around the beakdown volume[12]. A optical delay is introduced into the probe beam to image different time delays between the onset of breakdown and the propagation of the shock wave around the beakdown region. If focus is kept at breakdown volume then the shock wavefront and the wall of the initial cavitation bubble will both appear as dark lines on a field brightly illuminated by the probe pulse and the spherical shock waves appear as dark rings, see figure 2.3.

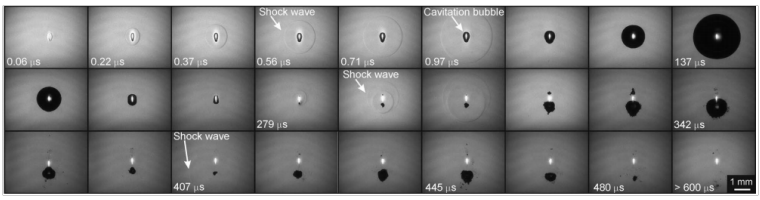

Figure 2.3: Shadow photography images of a laser induced cavitation bubbles expansion and collapse event. [29].

Due to the compressive pressure wave which causes a change in the efractive index of the liquid a dark wavefront appears on the image. Again the change in refractive index is sufficient to cause deflection of the illuminating light away from the imaging aperture alongwith the refractive index difference between the liquid and the bubble cavity causes deflection of the illuminating light. The average velocity of the shock wave is can be measured by dividing the distance between the center of the plasma and the dark ring i.e. the shock wave propagation distance by the time between the pump pulse and probe pulse which is set by the optical delay. The temporal resolution is determined by the pulse duration of the probe beam, and the spatial resolution is determined by the optics of the imaging system.

Petkovsek et al. [29] used shadow photoghraphy as a comparative method to study the dynamics of laser induced cavitation bubble. Here Probe Beam Deflection(PBD) was used to simultaneously measure the shock wave and maximum radius of cavitation bubble and hence compared it with shadow photography result. Comparision shows that the two type of method are in good agreement with each other. The maxium cavitation bubble radius they have measured was 0.5 mm to 1.5 mm.

Gregorcic et. al. [30] used PBD to study laser induced cavitation bubble oscillation and used shadow photoghraphy as a comparative method. It was found that data obtained in PBD was less as compared to shadow photoghraphy. The measured cavitation bubble radius was 0.2 mm. to 1.6 mm.

Shifferers et al. [31] used high speed shadow photoghaphy to visualise th bubble's shape in it's collapse phase. Here, a sequence of image used to visualise the collapse of a single bubble in front of a boundary.

2.5.2 Schlieren Photography:

Schlieren photography is another photography technique which can be thought of as the complement of shadow photography. In shadow photography the primary light which is coming from the probe laser enters the camera aperture directly. But the deflected light due to pressure wave is rejected by spatial filter such as knife edge aparture placed infront of the camera. In schlieren photographs, the shock wave will appear as bright on a dark background.

A. Vogel et al. [17] reported a development of a sensitive high-resolution white light schlieren technique with a large dynamic range forthe investigation of ablation dynamics.Here they have developed a modified Hoffman contrast technique with a 12 ns pulsed incoherent extended white-light source that enables an easily interpretable visualization of ablation plumes with high resolution.

A. Vogel et al. [18] used schlieren photghraphy to image the laser induced cavitation bubble collapse near a rigid boundary. Maximum bubble radius reported by them was 3.9 mm.

2.5.3 Streak Cameras:

Streak cameras convert a one-dimensional spatial image received over a duration of time into a two-dimensional image which is a function of both space as well as time. In this imaging methode the photocathode of a streak tube converts incident photons into a stream of photoelectrons which are passed through parallel deflecting plates. The number of electrons in the stream is directly proportional to the intensity of the light striking the photocathode. The direction in which the photoelectrons travel is determined by the voltage applied to the deflecting plates. If a ramp voltage applied across the deflecting plates, the photoelectrons are swept across one axis of a microchannel plate, which is the direction of propagation normal to both the slit and the time axes. The microchannel plate amplifies the signal and sends the photoelectrons to a phosphor screen, which converts the photo-electrons back to photons. These can then be imaged on film or on a CCD array.

Streak imaging of shockfront has two advantages over shadow or schlieren photography. First an image of the initial shock wave and cavitation bubble growth, after laser induced breakdown can be obtained for each laser pulse. This in fact eliminates the necessity to piece together the data on initial velocity from a number of images.

Besides that pulse duration, spot size, pulse energy effects the measurement. The second advantage is that by streak imaging one can measure the exact moment when the shock front separates from the cavitation bubble and from the plasma.

J.E. Chomas et al[32]. used streak camera optical imaging technique to observe bubble radial oscillations in order to understand the mechanisms of bubble destruction and predict the received echo from a bubble. They have used a high-speed streak camera with temporal resolution of 500 ps for the observation. K.E. Morgan et al.[33] used a high speed digital camera capable of 100 million frames/s for observation of micobubble evolution in a saline bath. They have only repoted the streak images in their paper and claimed that streak image is converted to a radius-time curve in Matlab by measuring the diameter at each time using a threshold criterion. The temporal resolution of the streak image repoted approximately 10 ns, and the spatial resolution is 0.12 μm per pixel.

R.Pecha et al.[34] claimed to measure directly for the first time the shape of a short light pulses emitted from a single air bubble trapped in a resonant sound field with a streak camera.

2.5.4 Interferometry:

Interferometry has also been used to characterize the pressures developed in liquids surrounding laser-induced breakdown sites. B. Ward and D.C. Emmony[19] have used four sequences of Mach-Zehnder inteferograms for study of pressure developed surrounding the cavitation bubble due to IR laser induced breakdown in water.Using this technique the maximum cavitation bubble radius they have measured 1 mm[19] The illuminating (probe) light is passed through a Mach-Zehnder interferometer, with the cuvette of liquid in which the pump laser is focused set on one arm of the interferometer and a compensating cuvette on the other arm. The probe beam has a short pulse duration, and hence, a short coherence length, so that the fringes can be localized at the focal plane of the pump laser. The radial pressure profiles due to acoustic transients in the liquid surrounding the focal point can then be obtained using the fringe-shift from the unperturbed water in the second cuvette. The main advantage of using interferometry is that the entire pressure profile, rather than simply the amplitude of the shock front, can be measured.

Cavitation bubble growth and oscillation are typically measured by optical techniques similar to those used to measure shock wave propagation. For example, initial cavitation bubble dynamics can be imaged with time-resolved photography as mentioned above. However, for measurement of the maximum bubble radius and cavitation bubble oscillation,microsecond time scales are needed, corresponding to optical delay lines kilometers in length. Electronic means are therefore used to create microsecond delays between the pump beam and probe beam. For imaging shock wave propagation, the same pulse is often used as the pump beam and the probe beam. For example, Vogel et.al.[13]used a 1064 nm pump beam and a frequency doubled 532 nm probe beam split from the pump beam. This technique eliminates any problems with trigger jitter between the pump and probe pulses. In contrast, since the trigger timing requirements are not as stringent when imaging cavitation oscillations, a larger variety of sources can be used for the probe beam, such as flashlamps, strobe lights, or dye lasers, or ever high-speed cameras (used in conjunction with the techniques listed above) have ideal frame rates (1×10^6 frames/sec.) for imaging cavitation bubbles.

2.5.5 Probe Beam Deflection Technique(PBDT):

PBDT is implemented by focusing probe beams through an enclosure filled with a propagation medium of the shock waves. After a cavitation bubble generation in the medium there is a change in refractive index due to the propagation of pressure waves. The probe beam de-

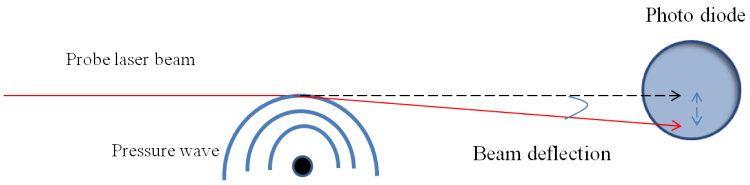

Figure 2.4: Beam dflection due to acoustic pressure wave.

flects and refracts as it interacts with the refractive index profile along its beam path, see figure 2.4. The probe beam deflection technique offers various advantages over transducer such as direct measurement of shock wave wavefront, low implimentation cost etc.

The main advantages of the PBDT over photography are as follows. With the PBDT one can observe all of the bubble's dynamics at one point in space. This means that with the help of probe beam signal

we can obtain information about the expansions, collapses, and shock waves etc. On the other hand, photography enables two-dimensional measurements from a single shot. In principle photoghraphy time resolution depends only on the pulse duration of the light source.

In recent years, the laser beam deflection probe has become a valuable tool for time resolved studies of shock [35, 36, 37, 38, 39] and acoustic [40, 41, 42], wave phenomena in fluids. The advantages of the laser probe detection include wide frequency bandwidth and dynamic range and, in contrast to conventional transducers, practically no influence on the probed field.

Gregorcic et al. [30] reported an optodynamic measurement of the laser-induced cavitation bubble and its oscillations based on a scanning technique using PBD. For data verification reasons, they simultaneously employed shadow photography during our experiments. The main goal of the study was to obtain measurements of the dynamics for the bubble oscillations using a laser beam-deflection probe and to compare them with shadow photography measurements. Petkovsek et al. [29] have presented measurements on laser-induced cavitation bubbles using a laser-beam deflection probe and shadow photography. The latter method was used for a comparison during the experiments and demonstrated the good agreement of both methods. The scanning technique based on the PBD and the time-evolution measurements based on the shadow photography produced measurement noise due to the repetition of the process. For this reason they developed a method based on an analysis of the secondary shock waves in order to reduce this measurement noise. This improved technique uses a unique property of PBD, all the cavitation bubbles oscillations and shock waves can be obtained from a single BDP signal. We showed that such a method significantly reduces the measurement noise, and as a result it can be used as an alternative to high-speed photography, which requires very sophisticated equipment.

Chapter 3

Cavitation Theory and Cavitation Bubble Dynamics Models

3.1 Basics of Cavitation:

Cavitation can be defined as a process involving formation of vapor phase of a liquid due to reduction in local pressure at constant ambient temperature. It is to be noted that the process of cavitation occurs only due to reduction of pressure at a particular region in the liquid and not due to the addition of heat to that particular region. However, various researchers have defined cavitation in many different ways.

Walton and Reynolds gave the following explanation about cavitaion [43] in a review about acoustically induced cavitation in water. They have taken the idea of tensile strength of water. Tensile strength of a material is defined as the amount of resistance generated in material to break it under tension. The theoretical tensile strength of water at room temperature is about 1000 atm (10^8 Pa)[43]. This implies that to generate acoustically induced cavitation in water by a sound pressure amplitude we need a pressure amplitude of at least 1000 atm. But in reality cavitation is observed with pressure amplitudes of about 1 atm and has been interpreted to imply the presence of pre-existing nuclei within the liquid [2]. A small free spherical bubble is the most simple nuclei that can be considered in any cavitation model. It is also known that a free bubble floats to the liquid surface and the gas that fills the bubble will diffuse out into the surrounding liquid medium. Epstein and Plesset [44] estimated that a 10 μm radius air bubble in air-saturated water will take about seven seconds to dissolve.

In reality a free bubble in a liquid is never completely in equilibrium. However, it has been assumed that the bubble is in equilibrium

in the considered cavitation model [45]. Furthermore the vapor pressure of the liquid is also neglected. After making these assumptions the following expression can be written for a perfect gas bubble in equilibrium in a liquid medium

$$P_g = P_\infty + \frac{2\sigma}{R_0} \tag{3.1}$$

where P_g is the gas pressure in the bubble, P_∞ the ambient liquid

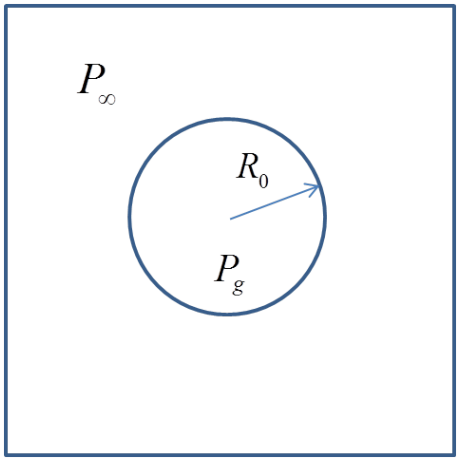

Figure 3.1: Spherical gas bubble in a liquid [45].

pressure, σ is the surface tension of the liquid and R_0 the equilibrium radius of the bubble. Thus

$$R_0 = \frac{2\sigma}{P_g - P_\infty} \tag{3.2}$$

If this value of bubble radius (R) is called the critical radius R_c then for stability

$$R_c = \frac{2\sigma}{P_g - P_\infty} \tag{3.3}$$

From equation (3.3) it is evident that if $R < R_c$, the term due to surface tension $2\sigma/R_0$ becomes more dominant leading to a bubble contraction, and if $R > R_c$, the gas pressure P_g term becomes more dominating causing a bubble expansion.

C.E. Brennen[46] while explaining cavitation reported that for a pure liquid, surface tension is the macroscopic manifestation of the intermolecular forces that tend to hold molecules together and prevent the formation of large holes in the liquid. If the liquid pressure, P,

exterior to a bubble of radius R, will be related to the interior pressure, P_B, by[46]

$$P_B - P = \frac{2\sigma}{R} \tag{3.4}$$

where σ is the surface tension. Here the surface tension (or, rather, surface energy) is assumed to be extended down to bubbles or vacancies of a few intermolecular distances in size. Ii is of interest to note that this approximation is found to be accurate [47]. Considering the temperature, T, to be uniform and the bubble contains only vapor, then the interior or internal pressure P_B will be the saturated vapor pressure $P_v(T)$. For equilibrium conditions, the exterior liquid pressure, $P = P_v - \frac{2\sigma}{R}$, will have to be less than P_v. Now if the exterior liquid pressure is maintained at a constant value just slightly less than $P_v - \frac{2\sigma}{R}$, the bubble expands and the excess pressure that initiates this bubble expansion will increase the bubble radius, and the internal pressure starts to fall. After the bubble attains the maximum size a further increase of the internal pressure will induce a the bubble to collapse.

To understand mathematically, let us consider the variation in pressure along the surface of a body immersed in a flowing liquid as given by Bernoulli's equation

$$P_1 + \frac{1}{2}\rho u_1^2 = P_2 + \frac{1}{2}\rho u_2^2 = H(constant) \tag{3.5}$$

Where, u is the velocity at a point where pressure P. We can see from this that

$$(u^2 + \frac{2P}{\rho})^{\frac{1}{2}} = (\frac{2H}{\rho})^{\frac{1}{2}} \tag{3.6}$$

If the liquid velocity u becomes greater than $(\frac{2H}{\rho})^{\frac{1}{2}}$, the pressure in an incompressible liquid has to be negative. As a result the liquid forms cavities that subsequently expands and releases this negative pressure.

3.2 Dynamical Equation of a Spherical Collapsing:

3.2.1 Empty Bubble:

Let us consider a spherical bubble of radius $R(t)$ and it's wall velocity $\dot{R(t)}$ at any instant t. Let us consider the fluid velocity $u(r,t)$ at an

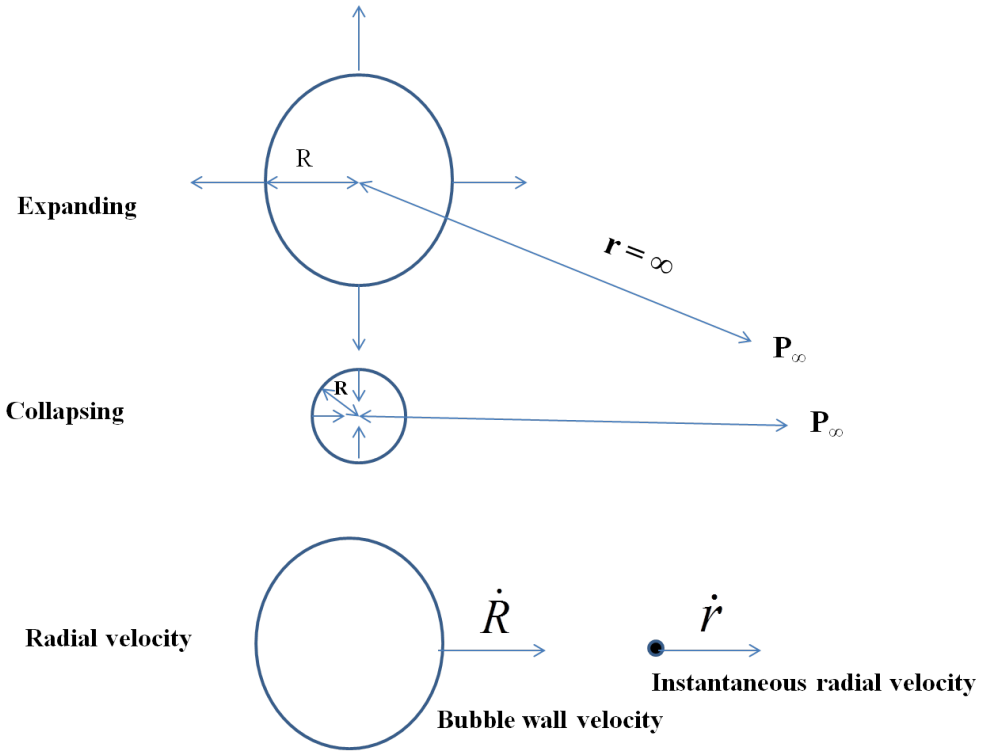

Figure 3.2: Expanding and collapsing spherical bubble [45].

instant of time t, at a range r falls as inverse square law with distance r as a result of the assumption of the incompressiblity of the liquid. Hence it follows that[46]

$$u(r,t) = R\dot{(}t)\frac{R^2(t)}{r^2(t)} \tag{3.7}$$

If the bubble radius changes from equllibrium bubble radius value R_0 to some other value, work is done on the bubble by the pressure, which exists at the center of the bubble. If P_∞ be pressure in the liquid far from the bubble then difference in work done by this pressure and that done by the pressure at the bubble wall P equals to the kinetic energyE_k in the liquid. Therefore we can write[1]

$$E_k = \frac{1}{2}\rho\int_{r=R}^{r=\infty}(4\pi r^2u^2)dr = 2\pi\rho R^3\dot{R}^2 \tag{3.8}$$

where ρ is the density of the liquid. Considering finite expansion of the bubble radius the above equation cam be written as[1]

$$\int_{R_0}^{R}(P - P_\infty)4\pi R^2dR = 2\pi\rho R^3\dot{R}^2 \tag{3.9}$$

After differentiating equation (3.9) w.r.t. $\dot{R}$, with keeping in mind

$$\frac{\partial\dot{R}}{\partial R} = 2\ddot{R} \tag{3.10}$$

The above equation reduces to

$$\frac{P - P_\infty}{\rho} = R\ddot{R} + \frac{3}{2}\dot{R}^2 \tag{3.11}$$

where P = pressure in the liquid at the bubble wall. Equation (3.11) called Rayleigh-Plesset equation of cavitation bubble dynamics.

3.2.2 Gas Bubble:

We now discuss the case of a gas filled bubble. The gas acts as a constraint and absorbs the energy of the liquid thereby shrinking in to stop the inward motion and eventually reverses the motion as shown in Figure 3.3. Suppose that the gas filling the bubble obeys the gas equation[45]

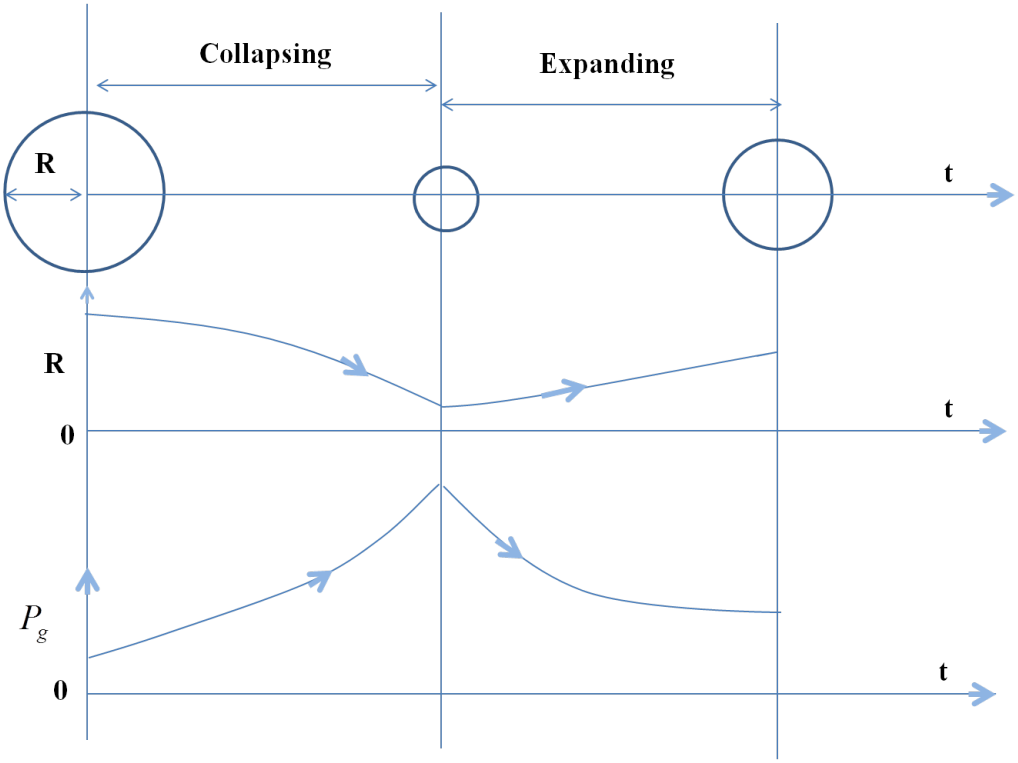

Figure 3.3: Schematic radius-time and pressure-time curves for a gas-filled spherical collapsing bubble[48].

$$P_g(\frac{4\pi}{3}R^3) = R_g T \tag{3.12}$$

where P_g is the gas pressure and R_g is the gas constant. And for an adiabatic changes,

$$P_g(\frac{4\pi}{3}R^3)^\gamma = constant \tag{3.13}$$

where γ is the ratio of the specific heats of the gas.
Suppose the initial gas content (at R = R_0) gives a gas pressure in the bubble of (P_0), where P_0 is the ambient pressure in the liquid . If the radius changes from R_0 to R at constant temperature, then gas pressure will be given by

$$P_g = (P_0)(\frac{R_0}{R})^{3\gamma} \tag{3.14}$$

Equation (3.11) then becomes

$$R\ddot{R} + \frac{3}{2}\dot{R}^2 = \frac{1}{\rho}[(P_0)(\frac{R_0}{R})^{3\gamma} - P_\infty] \tag{3.15}$$

where $P = (P_0)(\frac{R_0}{R})^{3\gamma}$

This equation was first derived and explored in many ways by Noltingk and Neppiras in their famous pair of papers of 1950 and 1951[45]. Poritsky[49] later introduced a term to include the effect of viscosity in the liquid. He showed that the viscous term arises in the boundary condition only, rather than through the Navier-Stokes equation[46].

3.2.3 Surface Tension and Vapor Pressure:

A correction for the pressure term, i.e. pressure at the bubble wall has also been done through the inclusion of pressure term (P_σ) due to surface tension $\frac{2\sigma}{R}$. The pressure at the bubble wall can be written as sum of the gas pressure(P_g) and vapour pressure(P_v), and Laplace pressure correction term due to surface tension(P_σ) as follows.

$$P = P_g + P_v - P_\sigma \tag{3.16}$$

If the gas pressure (P_g) is given by $(P_0 + \frac{2\sigma}{R_0} - P_v)(\frac{R_0}{R})^{3k}$, where k is the polytropic constant. Then pressure at the bubble wall takes the form

$$P = (P_0 + \frac{2\sigma}{R_0} - P_v)(\frac{R_0}{R})^{3k} + P_v - \frac{2\sigma}{R} \tag{3.17}$$

Substituiting this value of pressure in equation (3.11), we have

$$R\ddot{R} + \frac{3}{2}\dot{R}^2 = \frac{1}{\rho}[(P_0 + \frac{2\sigma}{R_0} - P_v)(\frac{R_0}{R})^{3k} + P_v - \frac{2\sigma}{R} - P_\infty] \tag{3.18}$$

3.2.4 Viscous Pressure Correction Term:

Another major factor that significantly influences the radial motion of a bubble is the viscosity of the liquid medium in which the bubble propagates. Also the bubble dynamics is incomplete without the viscosity correction term $\frac{4\mu\dot{R}}{R}$ in bubble dynamics equation. Where μ is the kinematic viscosity of the liquid. After inclusion of viscosity correction term, the pressure at the bubble wall takes the form

$$P = (P_0 + \frac{2\sigma}{R_0} - P_v)(\frac{R_0}{R})^{3k} + P_v - \frac{2\sigma}{R} - \frac{4\mu\dot{R}}{R} \tag{3.19}$$

Hence equation (3.11) becomes

$$R\ddot{R} + \frac{3}{2}\dot{R}^2 = \frac{1}{\rho}[(P_0 + \frac{2\sigma}{R_0} - P_v)(\frac{R_0}{R})^{3k} + P_v - \frac{2\sigma}{R} - \frac{4\mu\dot{R}}{R} - P_\infty] \tag{3.20}$$

Nowadays Eq.(3.11), (3.18), (3.20) all are called Rayleigh-Plesset's equation.

3.3 Equation Involving Compressibility of Liquid:

For faster bubble collapse, the compressibility of the liquid must be taken into account and the simplest step is to consider a constant stiffness of the liquid(i.e.constant sound velocity C in the liquid medium). This assumption is called is called the acoustic approximation and uses as the equation of state $\frac{dp}{d\rho} = C^2$ [4]. This approximation limits the analysis to the cases where the bubble wall velocity $\dot{R}$ is always small compared to C and incorporates the loss of energy by sound waves in cavitation bubble dynamics. Flynn [6] then showed that, if we neglect surface tension and viscosity, Eq. (3.11) yields with the help of acoustic approximation:

$$R\ddot{R} + \frac{3}{2}\dot{R}^2 = \frac{1}{\rho}[1 + \frac{\dot{R}}{C}][P + \frac{R}{C}(1 - \frac{\dot{R}}{C})\frac{dP}{dt} - P_\infty] \tag{3.21}$$

where P is the liquid pressure on the bubble wall. Herring [2] included a better description of the storage of energy through compression of the liquid as well as sound radiation, and obtained

$$(1 - \frac{2\dot{R}}{C})R\ddot{R} + (1 - \frac{4\dot{R}}{3C})\frac{3}{2}\dot{R}^2 = \frac{1}{\rho}[P + \frac{R}{C}(1 - \frac{\dot{R}}{C})\frac{dP}{dt} - P_\infty] \tag{3.22}$$

With the help of Kirkwood-Bethe[5] hypothesis Gilmore[4] gave a mathematically better approximated cavitation bubble dynamics equation. Kirkwood-Bethe hypothesis states that for a spherical wave of finite amplitude, the quantity $r\phi$ propagates with avelocity equal to the sum of the fluid velocity and local velocity of sound [4]. Where r= radial co-ordinate, and ϕ= velocity potential. According to Gilmore's assumption the bubble dynamics equation is given by

$$(1-\frac{\dot{R}}{C})R\ddot{R}+(1-\frac{\dot{R}}{3C})\frac{3}{2}\dot{R}^2=(1+\frac{\dot{R}}{C})H+\frac{R}{C}(1-\frac{\dot{R}}{C})\frac{dH}{dt} \quad (3.23)$$

where H is the difference in the liquid enthalpy between the bubble wall and infinity, and c is the velocity of sound of the bubble wall. Both H and C are functions of the motion of the bubble wall.

In another work, Keller and Kolodner [7] took into account the compressibility of water in the case of an underwater explosion when a bubble of gas is formed at high pressure. They have assumed that these bubbles expands rapidly until its pressure falls and becomes equal to that of the surrounding water, but inertia causes it to over expand. After the expansion stops, the pressure of the surrounding water compresses it again to a high pressure. This cycle of expansion and contraction continues with the maximum amplitude diminishing after every complete oscillation. If the water is treated as incompressible [50] then theory yields undamped oscillations of constant period. However, by treating the water as slightly compressible, Keller and Kolodner [7] predicted damped oscillations with diminishing period.

The effect of compressiblity in cavitation bubble wall motion is damping in variation of radius w.r.t. time. The damping in equation of bubble wall motion happens due to mainly three reasons:(1) Radiation damping, (2)Viscous damping, (3)Thermal damping [45].

(1)Radiation damping: Due to the oscillation of a spherical bubble a spherical wave generates. Thereby a loss of energy through sound radiation happens. That energy is lost can be seen from the fact that the pressure in the spherical wave at the bubble surface has a component in phase with the particle velocity [51].

(2)Viscous damping: Mallock [52] gives us a physical picture of the effect of viscosity on a pulsating bubble by considering a small element of a spherical shell of liquid at the liquid surface. This element has definite radial and lateral dimensions at the instant the bubble radius is at its equillibrium position. When the bubble expands, the small

liquid element is distorted, while at same time the radial thickness decreases and the lateral dimension increases. He also claimed that if we assume the liquid is in-compressible, that distortion is not caused by a change in volume but by viscous stresses. Hence as a result more energy is required to compress the bubble than is regained in the subsequent expansion.

(3)Thermal damping: For the case of a real bubble, a gas in contact with the liquid closely follows the isothermal equation of state since the liquid has a large specific heat and thermal conductivity. In the center of a real bubble away from a substance having a high specific heat, the gas nearly follows an adiabatic equation of state. Therefore, the thermal process is polytropic for a real bubble and there exist a phase difference between the increase in pressure per unit original pressure and the decrease in volume per unit original volume. This phase difference causes a hysteresis type effect. The work done on the gas volume by the driving pressure during compression is more than the work done by the internal gas in moving the surrounding liquid during expanion. This difference in the work done represents a net flow of heat into the liquid [51].

3.4 Different Cavitation Bubble Dynamics Model:

A number of bubble dynamics model, such as Rayleigh's model, Herring's model, Gilmore's model, Flynn's model, Keller-Miksis's model, have been proposed to describe the cavitation bubble dynamics in a liquid medium. Recent study of cavitation and cavitation collapse for the models confirm the fact that qualitative behavior of the models is essentially the same and the models do differ quantitatively [53].

3.4.1 Rayleigh-Plesset's Model:

This model is applicable for describing bubble evolution in an incompressible liquid. This model includes the zero order acoustic approximation. According to this model the bubble wall motion is given by [54]

$$R\ddot{R} + \frac{3}{2}\dot{R}^2 = \frac{1}{\rho}(P - P_\infty) \tag{3.24}$$

The dot represents differentiation with respect to time. Pressure at the bubble wall can be written as [55]

$$P = P_g + P_v - \frac{2\sigma}{R} - \frac{4\mu\dot{R}}{R} \tag{3.25}$$

If we assume that gas inside the bubble is a ideal gas and it is obeying polytropic process then pressure due to gas inside the bubble (P_g) can be written as [54]

$$P_g = P_0(\frac{R_0}{R})^{3\gamma} \tag{3.26}$$

Where γ = specific heat ratio. Now equation (3.25) takes the form

$$P = P_0(\frac{R_0}{R})^{3\gamma} + P_v - \frac{2\sigma}{R} - \frac{4\mu\dot{R}}{R} \tag{3.27}$$

Hence equation (3.24) becomes

$$R\ddot{R} + \frac{3}{2}\dot{R}^2 = \frac{1}{\rho}(P_0(\frac{R_0}{R})^{3\gamma} + P_v - \frac{2\sigma}{R} - \frac{4\mu\dot{R}}{R} - P_\infty) \tag{3.28}$$

Equation (3.28) is also known as Rayleigh-Plesset equation for cavitation bubble dynamics. Loshe et al.[56] have modified cavitation bubble dynamics equation described by Rayleigh-Plesset equation as

$$R\ddot{R} + \frac{3}{2}\dot{R}^2 = \frac{1}{\rho}(P - P_\infty) - \frac{2\sigma}{R\rho} - \frac{4\mu\dot{R}}{R} + \frac{R}{\rho C_\infty}\frac{d}{dt}P \tag{3.29}$$

with a Van der Waals type pressure

$$P = (P_0 + \frac{2\sigma}{R_0})(\frac{R_0^3 - h^3}{R^3 - h^3}) \tag{3.30}$$

where $h = \frac{R_0}{8.86}$ if the gas inside the bubble is argon.

3.4.2 Herring's Model:

C. Herring [2] developed a theory of the pulsation of gas bubble produced by an underwater explosion and reported a mathematical model about bubble dynamics. The essential features of the pulsation phenomenon is that an explosion creates a cavity filled with high pressure gas, which pushes the water radially outward against the opposing external hydrostatic pressure. The high velocity thus imparted to the

water causes it to outrun the equilibrium radius at which internal and external pressures are equal, and when the external pressure finally succeeds in bringing the expansion to a halt a contraction sets in, which again outrun and recompresses the gas to a high pressure. This phenomenon of oscillation may be repeated a number of times, until the original energy has become dissipated in one way or another. At each compression the high pressure developed gives rise to an acoustic impulse which even can be heard at a distance. This model based on the so called first order acoustic approximation, which assumes a constant velocity of sound in liquid, i.e. $C = C_\infty =$ constant.

The equation of bubble wall motion is given by [54]

$$R\ddot{R}(1 - 2\frac{\dot{R}}{C_\infty}) + \frac{3}{2}(1 - \frac{4}{3}\frac{\dot{R}}{C_\infty}) = \frac{1}{\rho}[P - P_\infty + \frac{R}{C_\infty}\dot{P}(1 - \frac{\dot{R}}{C_\infty})] \quad (3.31)$$

This model is siutable for small and moderate amplitude of oscillation when flow velocities are small [54].

3.4.3 Flynn's Model:

It is very similar to Rayleigh-Plesset model, taking into account compressibility in the near field but still in-compressible in far field. Fynn in his paper [6] constructed a mathematical formulation that enables us to study the effects of heat conduction, shear viscosity, compressibility, and surface tension on their dynamical behavior. The formulation is a large amplitude one in that it is specifically designed to describe the motion of a bubble that expands to some maximum radius and then contracts violently.

The formulation is used mainly to study the simultaneous effects of heat conduction, shear viscosity, and compressibility on the dynamics of bubbles. Infact all three of these effects are commonly called dissipative in the sense that they damp the motion of a freely pulsating bubble. It has claimed that heat conduction in general increases the violence of bubble motions, while shear viscosity and compressibility decrease it. In many instances, this competition between the effect of heat conduction and the effects of shear viscosity and compressibility makes it unrealistic to study the effect of heat conduction alone [6].

Here veloity of sound is constant in the liquid i.e. $C = C_\infty =$

constant. The bubble wall motion can be expressed as

$$\rho[R\ddot{R}(1-\frac{\dot{R}}{C_\infty})+\frac{3}{2}(1-\frac{1}{3}\frac{\dot{R}}{C_\infty})]=(1+\frac{\dot{R}}{C_\infty})(P-P_\infty)+\frac{R\dot{P}}{C_\infty}(1-\frac{\dot{R}}{C_\infty}) \tag{3.32}$$

here P = pressure at the bubble wall is given by equation (3.27).

3.4.4 Keller-Miksis's Model:

This model is based on large amplitude forced oscillation of a free bubble in a sound field [55]. It takes into account compressibility of the liquid, contant velocity of sound in liquid i.e. $C = C_\infty$ = constant. According to this model bubble wall motion is given by

$$R\ddot{R}(1-2\frac{\dot{R}}{C_\infty})+\frac{3}{2}(1-\frac{1}{3}\frac{\dot{R}}{C_\infty})=\frac{1}{\rho}[(1+\dot{R})(P-P_\infty)+\frac{R\dot{P}}{C_\infty} \tag{3.33}$$

Here P= pressure at the bubble wall is given by equation (3.27).

3.4.5 Gilmore's Model:

Gilmore [4] generalized the analysis to include higher order compressibility terms, and also the effects of viscosity and surface tension. With the help of Kirkwood-Bethe [5] hypothesis for equation of state of a liquid, in this model the velocity of sound in the liquid C, varies with the pressure P as

$$C=C_\infty(\frac{P+B}{P_\infty+B})^{\frac{n-1}{2n}} \tag{3.34}$$

Where $C_\infty=\sqrt{n\frac{(P_\infty+B)}{\rho}}$

Here B and n are constants which depends upon the particular liquid under consideration (for water $B \approx 3000$ atm and $n \approx 7$). A further quantity occuring in this model is an enthalpy difference between the liquid at pressure P an P_∞ under isentropic condition. The enthalpy difference, H, equals

$$H=\frac{1}{\rho}\frac{n}{n-1}(P_\infty+B)[(\frac{P+B}{P_\infty+B})^{\frac{n-1}{n}}-1] \tag{3.35}$$

Here P= pressure at the bubble wall is given by equation (2). The equation of bubble wall motion in Gilmore model then can be expressed as

$$R\ddot{R}(1-\frac{\dot{R}}{C})+\frac{3}{2}\dot{R}^2(1-\frac{\dot{R}}{3C})=H(1+\frac{\dot{R}}{C})+\frac{\dot{H}}{C}R(1-\frac{\dot{R}}{C}) \tag{3.36}$$

Chapter 4

Simulation Result

4.1 Bubble Dynamics Models: Compressibility vs Incompressibility

4.1.1 Comparison of Different Bubble Dynamics Model:

At the very beginning, we compare the time evolution of bubble radius, numerically simulated using different models. The chosen models are Rayleigh-Plesset's model (Eq. 3.24), Herring's model (Eq. 3.31), Flynn's model (Eq. 3.32), Keller-Miksis's model (Eq. 3.33), Gilmore's model (Eq. 3.36). All the models except the Rayleigh-Plesset's model considers compressibility of liquid and Fig. 4.1 basically compares bubble dynamics of an incompressible liquid (Rayleigh-Plesset's model) to the bubble dynamics of a compressible liquid (Herring's model, Gilmore's model, Flynn's model etc.). The parameters employed for these simulations are $\rho = 1000$ Kg/m^3, $P_0 = 2 \times 10^5$ Pa, $R_0 = 5 \times 10^{-6}$ m, $\gamma = 1.13$, $P_v = 2330$ Pa, $\sigma = 72.5 \times 10^{-3}$ N/m, $\mu = 8.9 \times 10^{-7}$ m^2/s, $B = 3.0398 \times 10^8$ Pa, $n = 7$, $C_\infty = 1498$ m/s and $R(0) = 0.01 \times 10^{-6}$ m, $\dot{R}(0) = 30$ m/s respectively. The magnitude of the velocity of sound in water at 20°C is used as C_∞. It can be seen from Fig. 4.1 that the time evolution of bubble radius obtained from Rayleigh-Plesset's model(blue curve) is substantially different from that of Keller-Miksis's model. It is to be noted that the nature of variation of bubble radius with time, obtained from different models that takes into account compressibility of liquid, is almost same and are superimposed in Fig. 4.1. Only the yellow line, depicting the time evolution of a bubble using the Keller-Miksis's model, is visible. The oscillation time for bubble evolution described by the incompressible model is higher than that of the compressible model and also the maximum radius attained during a particular oscillation

is significantly higher for the incompressible liquid.

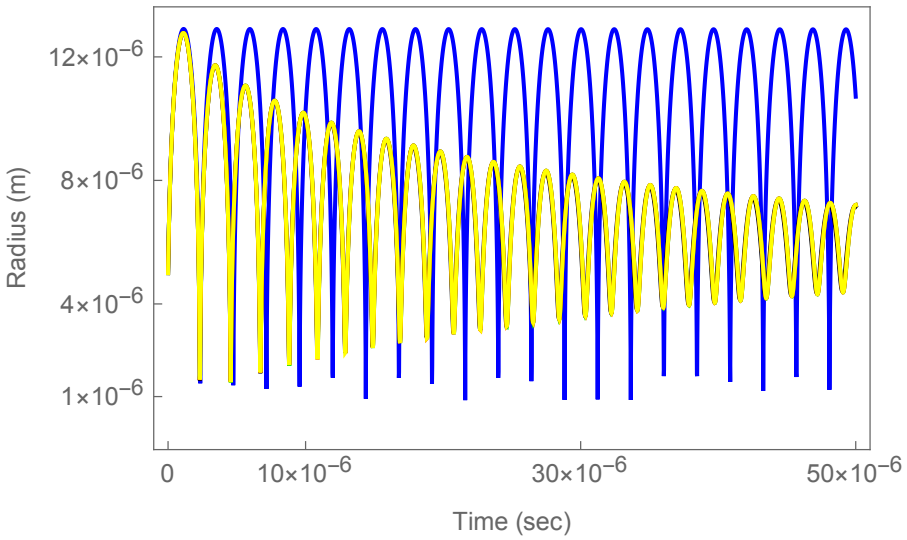

Figure 4.1: Comparison of the time evolution of bubble radius for an incompressible liquid simulated using Rayleigh-Plesset's model(blue curve) to that of a compressible liquid simulated using different models like Gilmore Model's(black curve), Flynn's(green curve), Herring's(red curve),Keller-Miksis's(yellow curve). The red, green, black lines are not visible because they are superimposed on each other.

Maximum Bubble Radius for Different Models During the First Oscillation:

The maximum bubble radius attained by the bubble during the first oscillation is plotted against initial bubble radius for the respective models considered in our work (Fig. 4.2). It has been found that all the models considered for this work gives almost the same value of maximum bubble radius at the first oscillation.

Maximum Bubble Radius for Different Models During Tenth Oscillation:

Fig. 4.3 depicts the variation of maximum bubble radius attained by the bubble during the tenth oscillation as a function of the initial bubble radius for each model. We find that for the tenth oscillation the variation of maximum bubble radius with change in initial bubble radius for an incompressible liquid (Rayleigh-Plesset's model) is significantly different from that of a compressible liquid calculated using the other models. It is to be noted that the variation of maximum bubble radius attained by the bubble during the tenth oscillation as a

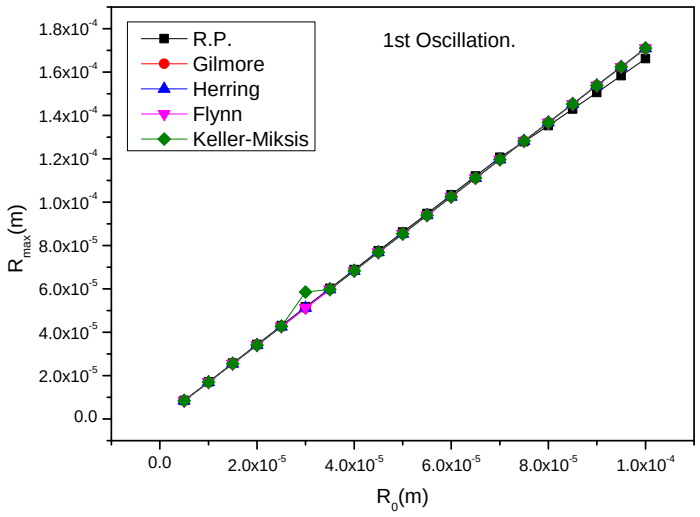

Figure 4.2: Plot for maximum bubble radius as a function of initial bubble radius during first oscillation for Rayleigh-Plesset's(black line), Gilmore's Model(red line), Flynn's(pink line), Herring's(blue line), Keller-Miksis's(green line).

function of the initial bubble radius is similar for all the models that take liquid compressibility into consideration.

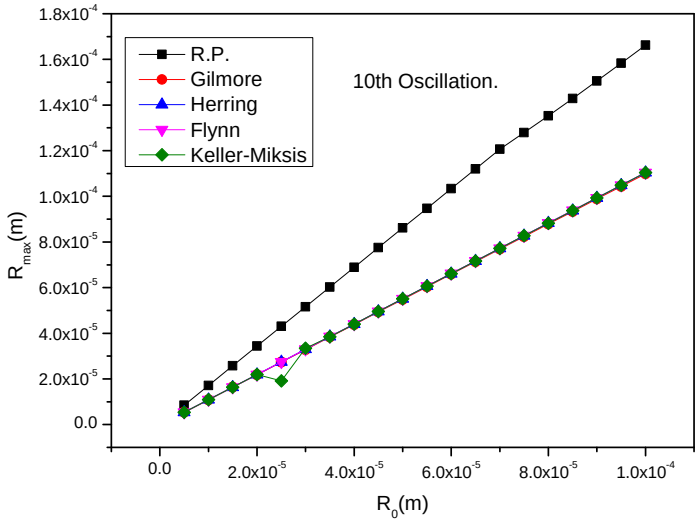

Figure 4.3: Plot showing maximum bubble radius as a function of initial bubble radius during tenth oscillation for Rayleigh-Plesset's(black line), Gilmore's Model(red line), Flynn's(pink line), Herring's(blue line), Keller-Miksis's(green line).

4.1.2 Comparison Between Rayleigh-Plesset's and Gilmore's Model:

To study the effects of the compressibility of the liquid medium on the temporal evolution of a bubble we compare the bubble dynamics in an incompressible liquid medium to the bubble dynamics in a compressible liquid medium. For this we choose Rayleigh-Plesset's model and Gilmore's Model(because mathematically it is better approximated and takes into account most of the major physical process)to describe the cavitation bubble dynamics in an incompressible and compressible liquid medium respectively.
In this simulation work water is taken as liquid medium for bubble evolution. Here we numerically solve Eq.(3.24) for the Rayleigh-Plesset's model and Eq.(3.36) for the Gilmore's Model respectively. The employed parameters for this comparative study are $\rho = 1000$ Kg/m^3, $P_0 = 2 \times 10^5$ Pa, $R_0 = 10 \times 10^{-6}$ m, $\gamma = 1.13$, $P_v = 2330$ Pa, $\sigma = 72.5 \times 10^{-3}$ N/m, $\mu = 8.9 \times 10^{-7}$ m^2/s, $P_\infty = 4 \times 10^5$ Pa, $B = 3.0398 \times 10^8$ Pa, $n = 7$. The boundary conditions for the simulation are $R(0) = 0.01 \times 10^{-6}$ m, $\dot{R}(0) = 30$ m/s. It is clear from figure 4.4 that the bubble collapses faster in a compressible liquid medium thereby indicating that the compressibility of the liquid medium is a crucial factor in bubble dynamics and can significantly modify the time evolution of a generated bubble in the liquid medium.

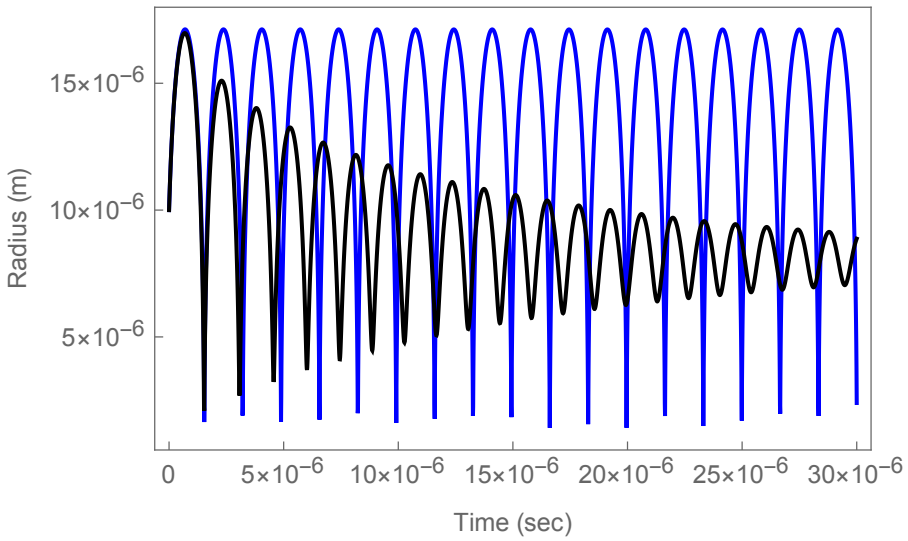

Figure 4.4: Comparison of Rayleigh-Plesset (blue curve) and Gilmore (black curve) Model.

4.1.3 Effect of Initial Bubble Radius on Maximum Bubble Radius for Gilmore Model:

We study the effect of initial bubble radius on the maximum radius that a bubble can attain using Gilmore model. We know that the ambient bubble pressure is a major factor that governs the cavitation bubble dynamics and may significantly influence the bubble dynamics. As a result we simulate maximum bubble radius vs initial bubble radius at different ambient pressures. Water is considered as liquid medium for bubble evolution. The employed parameters for this simulation of Eq. (3.36) are $\rho = 1000$ Kg/m^3 , $P_0 = 1 \times 10^5$ Pa, $R_0 = 5 \times 10^{-6}$ m, $\gamma = 1.13$, $P_v = 2330$ Pa, $\sigma = 72.5 \times 10^{-3}$ N/m, $\mu = 8.9 \times 10^{-7}$ m^2/s, $B = 3.0398 \times 10^8$ Pa, $n = 7$ with the boudary condition $R(0) = 0.01 \times 10^{-6}$ m, $\dot{R}(0) = 30$ m/s at fixed ambient pressure(P_∞). Fig. 4.5 shows a linear dependence of maximum bubble radius on initial bubble radius and is qualitatively similar at all ambient pressures. However, the plots at different ambient pressures vary quantitatively and for a fixed initial bubble radius increase of ambient pressure decreases the maximum bubble radius.

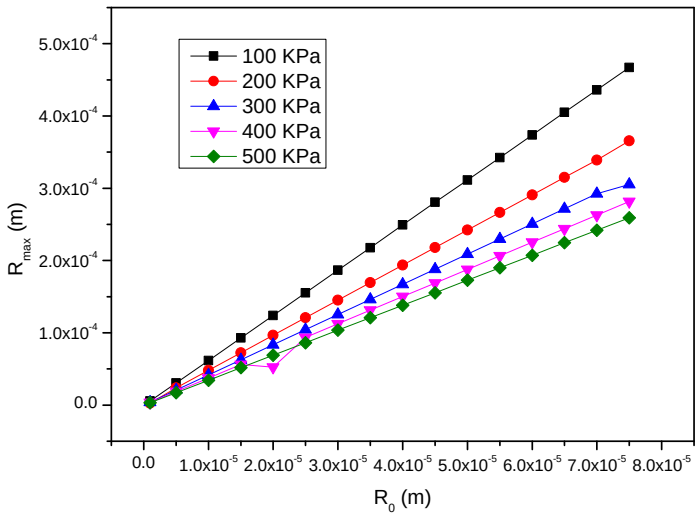

Figure 4.5: Maximum bubble radius with initial bubble radius plot for various ambient pressure.

4.1.4 Simultaneous Variation of Bubble Radius and Internal Pressure at Bubble Wall with Time:

From our simulated results we can infer that cavitation bubble radius oscillates about some equillibrium bubble radius value. To have an idea about how the internal bubble pressure changes during the time evolution of a bubble we have simultaneously plotted the internal bubble pressure and bubble radius as a function of time.
Here equation (3.29) has been simulated assuming Van der Waals type gas pressure inside bubble as given by equation (3.30). The numerical value of the used physical parameters are as follows $\rho = 1000$ Kg/m^3, $P_0 = 1 \times 10^5$ Pa, $\gamma = 1.13$, $P_v = 2330$ Pa, $\sigma = 72.5 \times 10^{-3}$N/m, $\mu = 8.9 \times 10^{-7}$ m^2/s for water and $\rho = 1175$ Kg/m^3, $P_0 = 1 \times 10^5$ Pa, $\gamma = 1.13$, $P_v = 2330$ Pa, $\sigma = 64 \times 10^{-3}$ N/m, $\mu = 1.420 \times 10^{-6}$ m^2/s for glycerin with the boundary condition $R(0) = 0.01 \times 10^{-6}$ m, $\dot{R}(0) = 30$ m/s.

The results are plotted for both water, Fig. 4.6, as well as glycerin, Fig. 4.7. It is evident that as the bubble radius increases internal

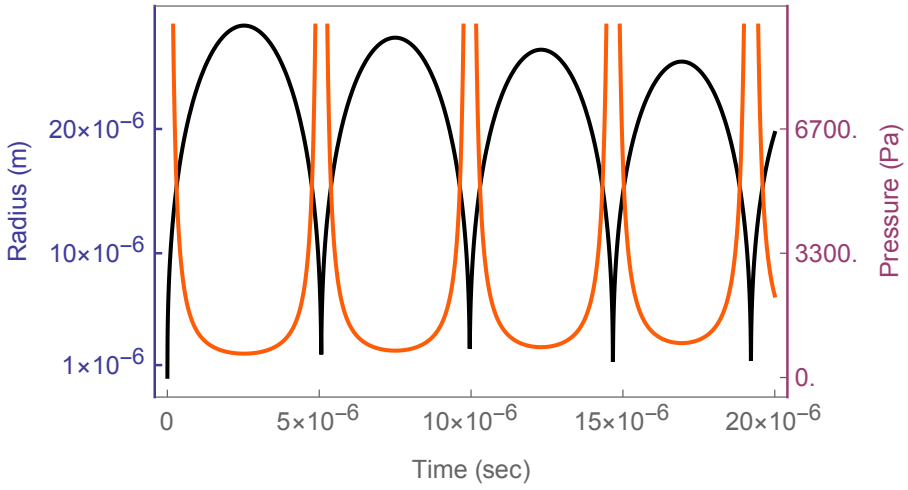

Figure 4.6: Simultaneous variation of internal bubble pressure at the bubble wall(orange curve) and bubble radius(black curve) with time for water as liquid medium.

pressure of the bubble decreases and vice versa. After a bubble attains its maximum radius the internal bubble pressure starts to rise thereby causing the bubble to contract and eventually collapse. This pattern is oscillatory in nature.

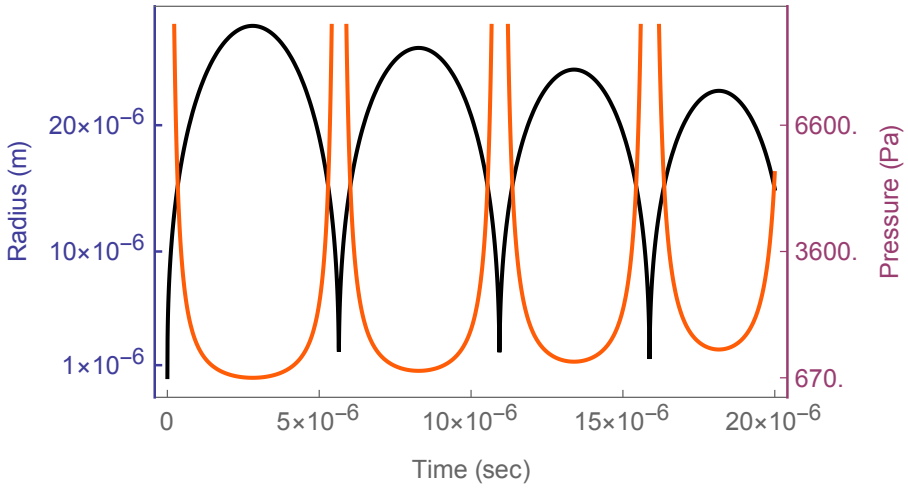

Figure 4.7: Simultaneous variation of internal bubble pressure at the bubble wall(orange curve) and bubble radius(black curve) with time for glycerin as liquid medium.

4.2 Parameter Optimisation of Rayleigh-Plesset's Model:

In this section we discussed the effects of different liquid properties like viscosity, density etc., as well as the other parameters that appears in the equation describing the Rayleigh-Plesset's model on maximum bubble radius. Here we have chosen Rayleigh-Plesset's Bubble dynamics equation given by Eq.(3.24). Ideal gas inside a bubble is an ideal case. Hence for the sake of more realistic case we have considered that the gas inside the bubble obeys a Van der Waals type gas equation.

4.2.1 Effect of Ambient Pressure on Maximum Bubble Radius:

As we already discussed ambient pressure is one of the major factor in time dependent bubble evolution. We were interested to see how ambient pressure effects maximum bubble radius. Here glycerine has been chosen as liquid medium for bubble evolution. Equation (3.24) has been numerically simulated with a Van der Waals type gas pressure inside the bubble given by equation (3.30). The employed parameters for this simulation are $\rho = 1175$ Kg/m^3, $P_0 = 1 \times 10^5$ Pa, $\gamma = 1.13$, $P_v = 2330$ Pa, $\sigma = 64 \times 10^{-3}$ N/m, $\mu = 1.420 \times 10^{-7}$m^2/s, $R(0) = 5 \times 10^{-6}$ m, with the boudary condition $R(0) = 0.01 \times 10^{-6}$ m, $\dot{R}(0) = 30$ m/s for fixed initial bubble radius($R(0) = 5 \times 10^{-6}$ m).

Figure 4.8 shows that as the ambient pressure increases the max-

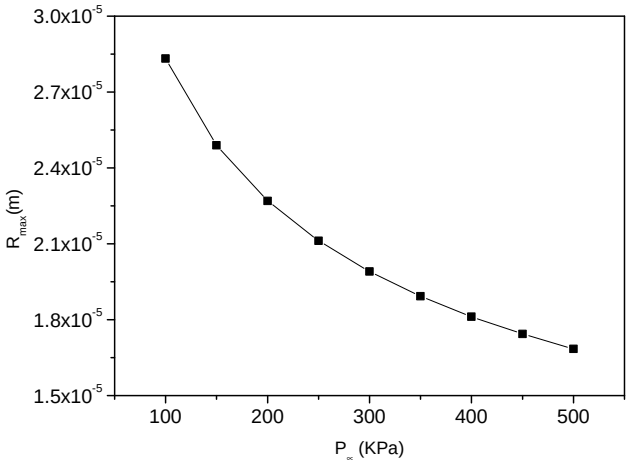

Figure 4.8: Maximum bubble radius as a function of ambient pressure plot for fixed initial bubble radius($R(0) = 5 \times 10^{-6}$ m).

imum bubble radius value decreases. The maximum bubble radius changes from a value greater than 2.7×10^{-5} m to less than 1.8×10^{-5} m as ambient pressure changes from 100 KPa to 500 KPa. This nature of variation of maximum bubble radius against ambient pressure has also been tested for different initial bubble radius like 5×10^{-6}, 10×10^{-6}, 15×10^{-6} and $20 \times^{-6}$ m etc, and the results are presented in Fig. 4.9. It is clear the nature of variation of maximum bubble radius with ambient pressure, for other initial bubble radius, are identical.

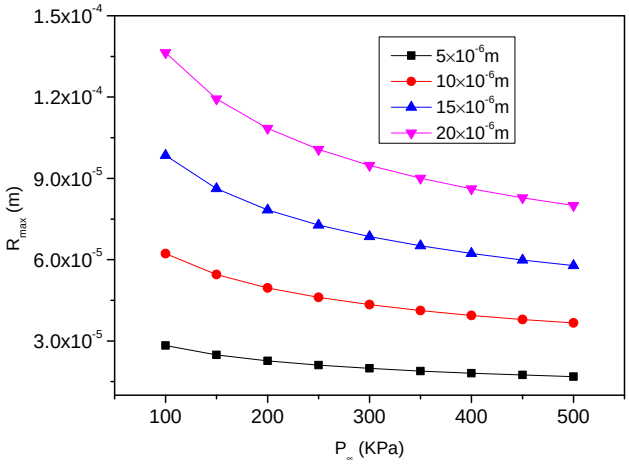

Figure 4.9: Variation of maximum bubble radius with ambient pressure for different initial bubble radius.

4.2.2 Effect of Initial Bubble Radius on Maximum Bubble Radius:

Variation of maximum bubble radius with initial bubble radius has also been studied through numerical simulation. Here equation (3.24) has been numerically simulated with a Van der Waals type gas pressure inside the bubble given by equation (3.30). Glycerine has been taken as liquid medium for bubble evolution. The employed parameters are $\rho = 1175$ Kg/m^3, $P_0 = 1 \times 10^5$ Pa, $\gamma = 1.13$, $P_v = 2330$ Pa, $\sigma = 64 \times 10^{-3}$ N/m, $\mu = 1.420 \times 10^{-7}$ m^2/s, with the boudary condition $R(0) = 0.01 \times 10^{-6}$ m, $\dot{R}(0) = 30$ m/s at fixed ambient pressure. Figure 4.10 shows the simulation result.

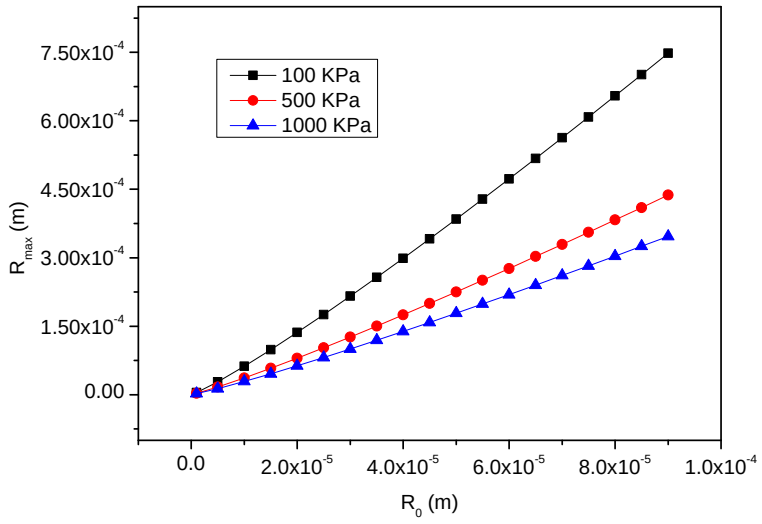

Figure 4.10: Maximum bubble radius with initial bubble radius plot at different fixed abmient pressure.

Figure 4.10 shows that for a fixed ambient pressure the maximum bubble radius increases linearly with increase initial bubble radius. This nature of variation of maximum bubble radius with initial bubble radius is also investigated for different ambient pressures like 100 KPa, 500 KPa, 1000 KPa. With increase in ambient pressure the slope of the line decreases. This implies that the maximum bubble radius reached by the bubble decreases with increase in ambient pressure.

4.2.3 Variation of Maximum Bubble Radius with Density of Liquid:

To study the effects of density of liquid on bubble dynamics we hypothetically assume that for a small change in liquid density other liquid properties like viscosity, surface tension etc remain constant. Here equation (3.24) has been numerically simulated with a Van der Waals type gas pressure inside the bubble given by equation (3.30) for both water and glycerin. The parameters for water are $P_0 = 1 \times 10^5 Pa$, $\gamma = 1.13$, $P_v = 2330Pa$, $\sigma = 72.5\times10^{-3}N/m$, $\mu = 8.9\times10^{-7}m^2/s$. The parameters for glycerin are $P_0 = 1 \times 10^5 Pa$, $\gamma = 1.13$, $P_v = 2330Pa$, $\sigma = 64 \times 10^{-3}N/m$, $\mu = 1.420 \times 10^{-6}m^2/s$. The initial boundary conditions for both water and glycerin are $R(0) = 0.01 \times 10^{-}6m$, $\dot{R}(0) = 30m/s$.

It can be seen from Fig. 4.11 (a) and (b) that with the increase in the density value the maximum bubble radius decreases. This nature is observed both for glycerin (Fig. 4.11 (a)) as well as for water(Fig. 4.11 (b)).

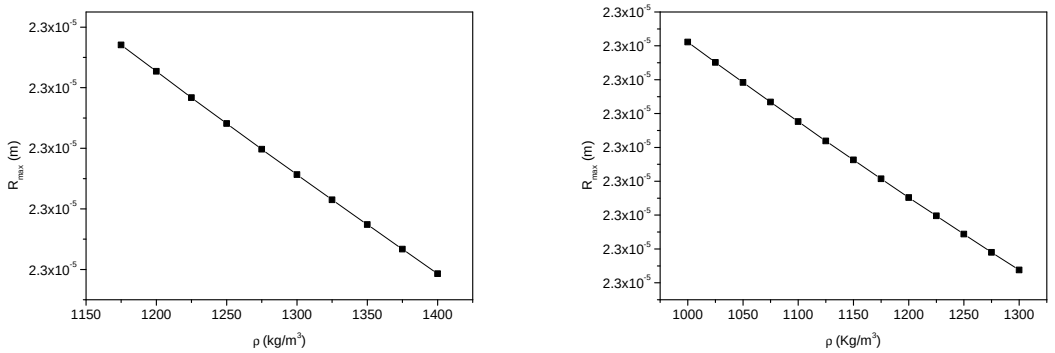

(a) Plot for glycerine.

(b) Plot for water.

Figure 4.11: Maximum bubble radius as a function of density plot for glycerine and water.

From figure 4.11 (a),(b) it can be seen that with the increase in density of the liquid the maximum bubble radius decreases. But this decrement is very small in bubble radius value. In figure 4.11 (a) the density varies from 1150 to 1400 Kg/m^3 but there is no change in the maximum bubble radius value upto first decimal point (it is fixed at 2.3×10^{-5}m). Similar insignificant change in maximum bubble radius value has been observed in the case of water also, see figure 4.11 (b).

4.2.4 Effect of Van der Waals Hard-core Radius (h) on Maximum Bubble Radius:

We study the effect of variation of Van der Waals hard-core Radius(h)on the maximum Bubble Radius. For this we numerically solve Eq. (3.24) with a Van der Waals type pressure inside the bubble given by Eq.(3.30) along with following employed parameters, $\rho = 1175Kg/m^3$, $P_0 = 1 \times 10^5 Pa$, $\gamma = 1.13$, $P_v = 2330Pa$, $\sigma = 64 \times 10^{-3}N/m$, $\mu = 1.420 \times 10^{-7}m^2/s$. The boundary condition is $R(0) = 0.01 \times 10^{-6}m$, $\dot{R}(0) = 30m/s$ at fixed ambient pressure. Glycerin is considered as liquid medium for bubble evolution. We know that Van der Waals hard-core radius is basically a correction term to the bubble radius. Fig. 4.12 shows that with the increase in the value of Van der Waals hard-core radius the maximum bubble radius increases. We also show the plots for the maximum bubble radius as a function of hard core radius at different ambient pressures (100 KPa, 200 KPa, 300 KPa, 400 KPa, and 500 KPa)in Fig. 4.13. We see a similar pattern like that of Fig. 4.12 at different ambient pressures.

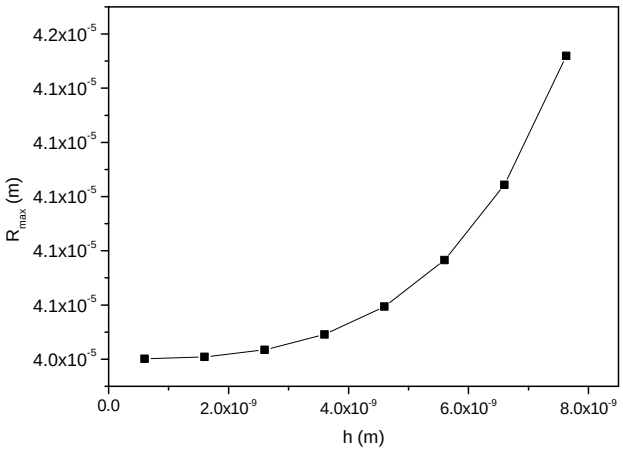

Figure 4.12: Maximum bubble radius as a function of Van der Waals hard-core radius(h) plot. Here ambient pressure is taken 100 KPa.

For this we numerically solve Eq. (3.24) using the following employed parameters, $\rho = 1175$ Kg/m^3, $P_0 = 1 \times 10^5$ Pa, $\gamma = 1.13$, $P_v = 2330$ Pa, $\sigma = 64 \times 10^{-3}$ N/m, $\mu = 1.420 \times 10^{-7}$ m^2/s. The boundary condition is $R(0) = 0.01 \times 10^{-6}$ m, $\dot{R}(0) = 30$m/s at fixed ambient pressure.

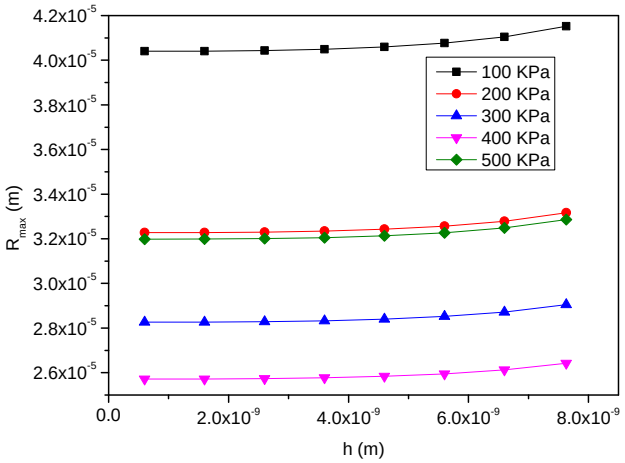

Figure 4.13: Comparison of maximum bubble radius vs Van der Waals hard-core radius plot for different ambient pressure.

Chapter 5

Optical Detection Technique

5.1 Optical Detection Technique

In this chapter we have discussed the experimental set up for detecting the bubble by PBD technique. This technique is based on deflection and absorption of probe beam when it interacts with bubble. The phenomenon of deflection occurs beacuse of the difference in refractive index of the medium inside and outside of the bubble. The deflection happens because the beam goes through refraction while passing the bubble. Snell's law will determine the angle of deflection. The absorption of light will be determined by Beer-Lambert law[57].

According to Beer-Lambert's law when a light ray of intensity I_0 goes through a medium of absorption coefficient α, an attenuation in intensity happens. The intensity after attenuation is given by[58]

$$I = I_0 e^{-\alpha l} \tag{5.1}$$

where l = path length travelled by the radiation in the medium.

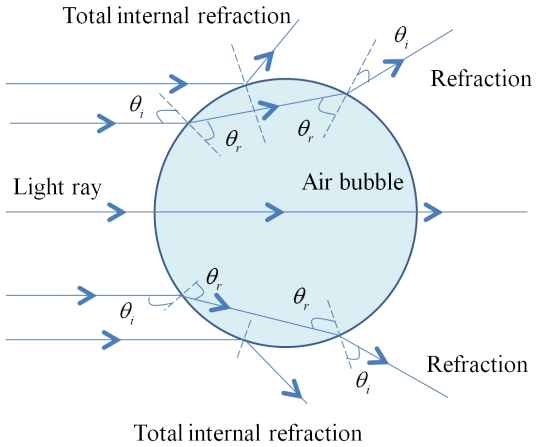

Figure 5.1: Projection of beam through medium having bubble. θ_i and θ_r are the angle of incidence and refraction respectively .

Also as a ray falling on a surface of a bubble at an angle θ_i with the normal at point of incidence, the angle of refraction θ_r can be calculated by Snell's law as[57]

$$\theta_r = \sin^{-1}\left(\frac{n_i \sin\theta_i}{n_r}\right) \tag{5.2}$$

where n_i = refractive index of incident medium and n_r = refractive index of refraction medium.

The intensity of refracted component is given by Fresnel's coefficient as[57]

$$T_{par} = 4\frac{\sin\theta_i \sin\theta_r \cos\theta_i \cos\theta_r}{\sin^2(\theta_i + \theta_r)\cos^2(\theta_i - \theta_r)} \tag{5.3}$$

$$T_{per} = 4\frac{\sin\theta_i \sin\theta_r \cos\theta_i \cos\theta_r}{\sin^2(\theta_i + \theta_r)} \tag{5.4}$$

where T_{par} and T_{per} are parallel and perpendicular components of refracted ray respectively. For our setup the total intensity observe by

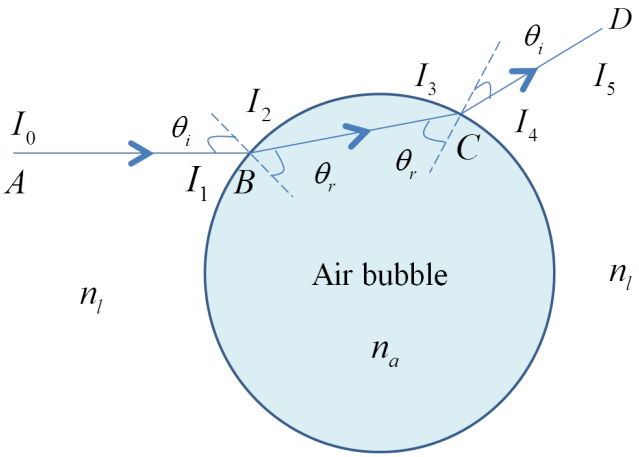

Figure 5.2: Deflection of light ray through an air bubble of refractive index n_a immersed in liquid medium of refractive index n_l.

photodiode will be given by the sum of the change in intensity due to Beer-Lambert's law and Fresnel's law of refraction intensity. Let us assume that a light ray of intensity starts from piont A with intensity I_0. After travelling a path length l_1 trough a medium of refractive index n_l it reaches point B as shown in Fig. 5.2. According to Beer-Lambert's law the intensity at point B just before refraction can be written as

$$I_1 = I_0 \exp(-\alpha_l l_1) \tag{5.5}$$

where α_l is the absorption coefficient of the liquid medium. At point B it goes through refraction. Let the angle of incidence is θ_i, and angle of refraction is θ_r. At point B just after refraction the intensity is I_2, then by Fresnel's law of refraction of intensity, considering only perpendicular component

$$I_2 = T_{per} I_1 \tag{5.6}$$

It is found that on avarage the difference between parallel and perpendicular component is less than 0.5 per cent [57]. Hence only the perpendicular component has been considered. Then the ray travells through the air bubble of path length l_2 and reaches the point C with intensity I_3. Hence the intensity I_3, just before refraction at point C can be written as

$$I_3 = I_2 \exp(-\alpha_a l_2) \tag{5.7}$$

where α_a is the absorption coefficient of air. If I_4 is the intensity just after refraction at point C, then

$$I_4 = T_{per} I_3 \tag{5.8}$$

And travelling through a path lenth l_3 it reaches a detector placed at point D with intensity I_5. Hence I_5 can be written as

$$I_5 = I_4 \exp(-\alpha_l l_3) \tag{5.9}$$

By successsive substitution of equation of Eq. (5.5), (5.6), (5.7), (5.8) in (5.9), it can be shown that

$$I_5 = I_0 T_{per}^2 \exp[-(\alpha_l l_1 + \alpha_a l_2 + \alpha_l l_3)] \tag{5.10}$$

where T_{per} is given by equation (5.4). Since T_{per} depends on θ_i the position of the bubble in the beam will play a major role. Because of the presence of deflection, QPD is use to observe the change in intensity. The beam deflection phenomenon and expected observation are as follows[59].

Quadrant Photodiode Concept: A quadrant detector is a silicon photo detector with four active photodiode areas. These detectors have the ability to measure extremely small changes in the position of a light beam and are used for detecting and measuring the position displacements.

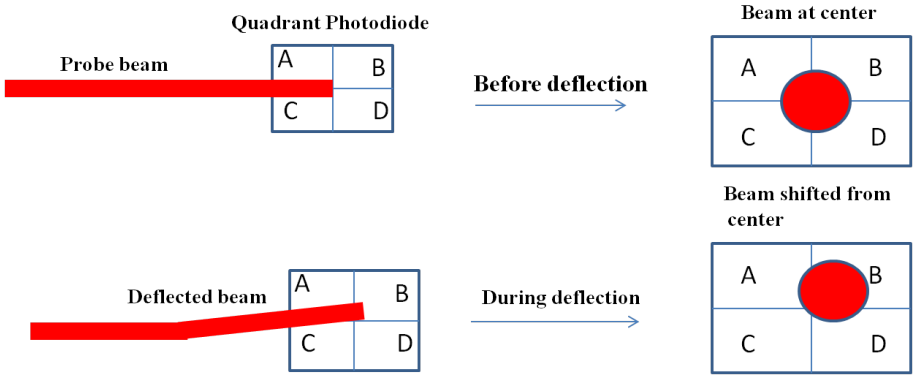

Figure 5.3: Schematic of probe beam deflection using QPD.

As shown in Fig. 5.3 by comparing the signal received from each of the four separate photodiodes, or quadrants, the position of the spot, relative to the centre of the device can be determined. X (horizontal displacement) and Y (verticle displacement) can be approximated by the relation

$$X = \frac{(A+C)-(B+D)}{A+B+C+D} \tag{5.11}$$

$$Y = \frac{(A+B)-(C+D)}{A+B+C+D} \tag{5.12}$$

where A, B, C and D are the signals generated from each of the quadrants. The time response of the signal as the bubble enters into the

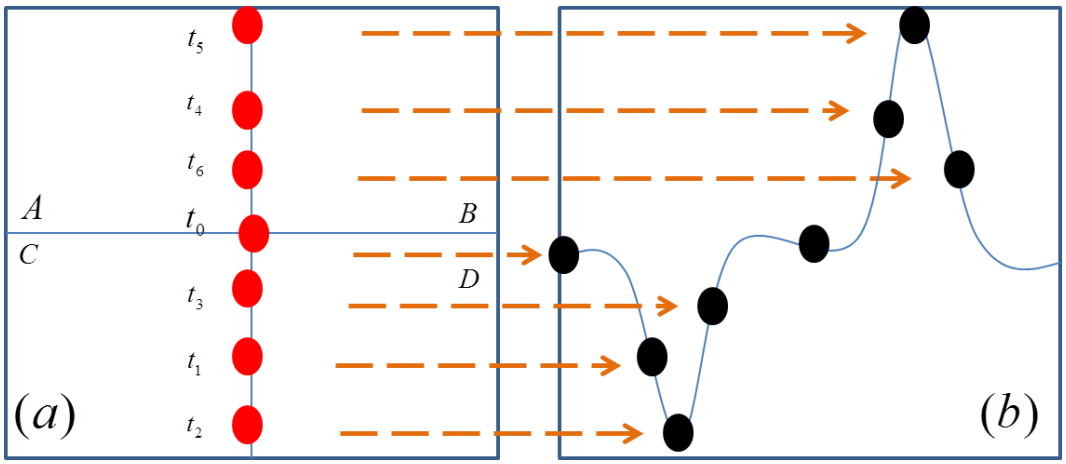

Figure 5.4: Beam deflection along the verticle and corresponding signal nature [59] . The beam spot position on QPD at different time (a) and the corresponding signal at oscilloscope (b).

beam path is shown in Fig. 5.4. In ours case since beam interacts with the air bubble perpendicularly, we don't expect any displacement in X direction. The position of deviated beam at different time is shown in Fig. 5.4 (a).

At time t_0, before the bubble enters into the beam the spot at photodiode will be at center and the intensity is given by $I_0 \exp(-\alpha l)$, where α and l would be determined by the medium (marked as zero level for futher discussion). At Time t_1 and t_2 the signal will deviate away from the photodiode and then it will come back at t_3 to zero level. Again at later time t_4 and t_5 it will deviate away from the photodiode and come back towards the center at time t_6. The recorded signal will have bipolar nature with negative and positive peak with reference to zero level as shown in Fig. 5.4(b). For detecting this type signal QPD would be ideal, but single photodiode can also give the same response given that the deflection is in one dimension as in our case.

The interaction of incident probe laser beam and air bubble can be considered as a combination of three consecuitive interaction moment as mentioned above. The reason for the bipolar nature of signal is as follows.

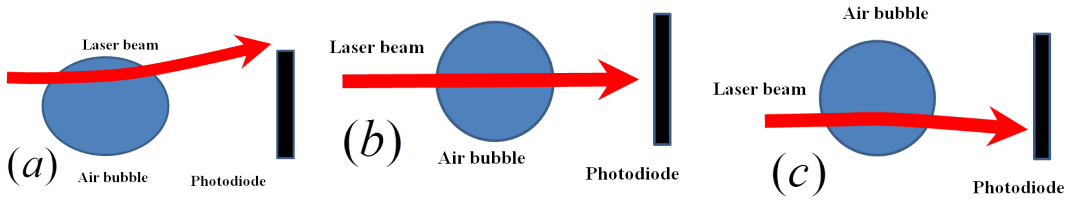

Figure 5.5: Schematic diagram showing the deflection of beam as bubble enters into beam (a), within the beam (b), and leaving the beam (c).

Position 1: Bubble Entering into Laser Beam Path: As the air bubble enters into the probe laser beam, θ_i is close to 48.6 degree which is the critical angle for water-air interface as per snell's law at angle above of close to 48.6 degree the angle of deviation of refracted beam will be large and make it to go off the photodiode as shown in Fig. 5.5 (a). As per equation (5.10) T_{per} would be very less and since all bubble is not in the beam exponential term of the equation would also be less. Hence, drop in photodiode signal would be observed.

Position 2: Bubble within Laser Beam Path: When majority of the air bubble surface will be in the beam, as shown in Fig. 5.5(b), θ_i will be close to 0 degree and hence absoprtion will dominate over T_{per} and the transmitted beam will follow Beer-Lambert's law. Hence the signal is expected to grow exponenetial to $I_0 \exp(-\alpha l)$ where α and l would be sum of air and liquid.

Position 3: Bubble Leaving Laser Beam Path: As the air bubble about to leave the beam, as shown in Fig. 5.5(c), the same situation as in Position 1 would happen. But in this case the deviated light will be directed towards the photodiode and hence enhanced photodiode signal is expected to be seen.

5.2 Experimental Arrangement

A PBD technique is designed to detect moving air bubbles in a liquid column as shown in Fig. 5.6. A 10 mm diameter glass column with a small hole of diameter 1 mm in the sintered material at the bottom is used as liquid column. An air pump is connected at the bottom of liquid column for a continuous flow air flow. Bubbles are generated by gas diffusion method[60, 61]. In this method air is released through nozzle and bubbles forms through the diffusion of air in liquid. By controlling the flow of air we managed to form the spherical single air bubble at time through a pinch off like process[62, 63, 64]. After the bubble detached from the hole it rises in liquid column due to buoyancy and collapses at the top of liquid column. A carefull observation of the air bubble production phenomena leads us to conclude that the produced air bubble at the bottom are initially nearly spherical but as it rises up it goes through a continuous shape deformation and tries to attain a ellptical shape. BESTO He-Ne laser at oprating wavelength

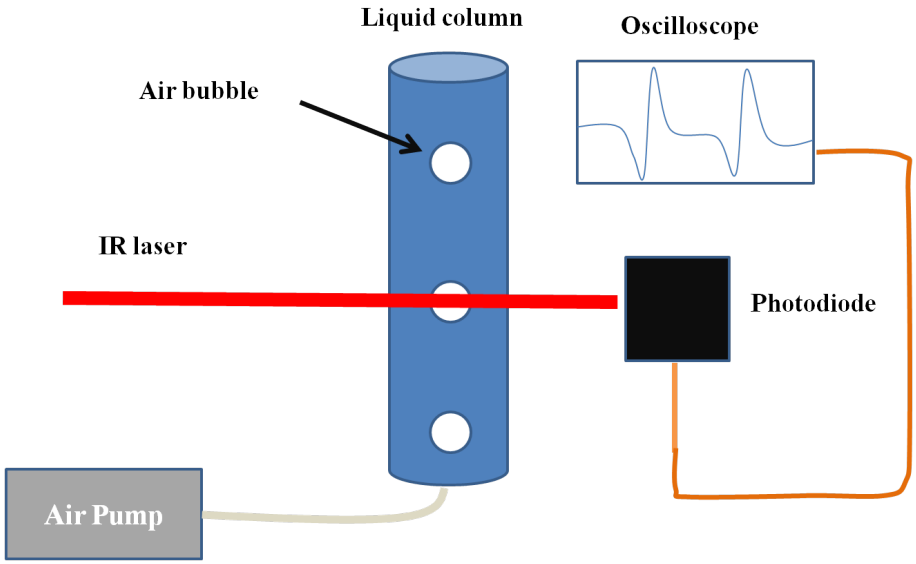

Figure 5.6: Schematic of experimental set-up.

of 632-8 nm having power of 5mW is been used as probe beam laser.

By changing the wavelength of the probe laser beam, as expected no observable changes were seen.

A fast photodiode [FDS010] having an active area of 0.8 mm^2 placed in line with probe beam is used to detect the air bubble flowing through the liquid column. DPO 3035 Digital Phosphor Oscilloscope [Tektronix] connected with the fast photodiode is been used to record the signal.

All the experiments have been performed in glycerine as well as in water. In glycerine the observed signal is smooth as compared to water as discussed in section 5.3. For the other experiment the data obtained for water is discarded and only the observation made for glycerine are discussed.

5.3 Result and Discussion

5.3.1 Effect of Different Liquid Medium

The observation made for the air bubble in glycerine and water is shown in Fig. 5.7 (a) and (b) respectively. As can be seen in both

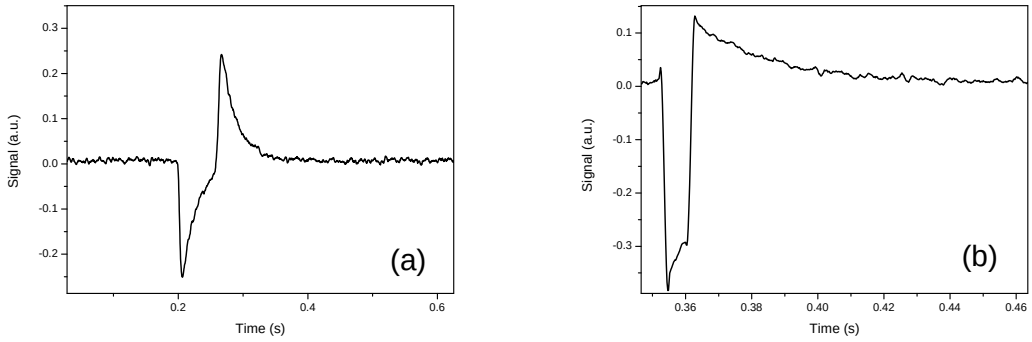

Figure 5.7: Observed signal for the air bubble propagating through pure glycerine (a) and water (b).

the cases bipolar feature is visible. In case of glycerine as can be seen the bipolar feature is symmetric in nature. Contrary to that in water although it is symmetric, a sudden jumps from negative to positive peak happens with small trace of exponential growth.

By fitting the exponential growth for both the cases with equation

$$y = A_0 \exp(t/\tau) + y_0 \tag{5.13}$$

we found that τ(glycerine)= 0.0235 s and τ(water)= 0.0042 s. The obtained value of τ indicates that movement of air bubble in water

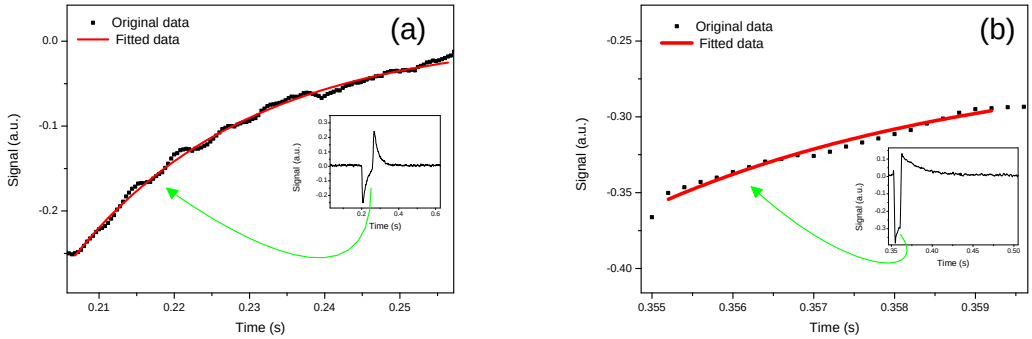

Figure 5.8: Measurement for exponential growth of observed signal for glycerine (a) and water (b) respectively. Black dotted curve is signal and red line is fitted curve.

is faster as compared to glycerine which is obvious glycerine being more viscous as compared to water. The sudden jump in the case of water indicates that the air bubble in water which moving faster as compared to glycerine spend less time in beam and hence not allowed to attain $I_0 \exp(-\alpha l)$ level.

5.3.2 Effect of Different Probe Beam Diameter

From the previous observation it is been concluded that if air bubble is allowed to spend more time in beam, symmetric nature of the bipolar feature can be attained. For this purpose experiment is been performed for different beam size. A bi-convex lens if focal length 100 mm is used to focus the probe beam. By varing the position of liquid column in different focal plane, the different beam size is attained. For this experiment medium used is glycerine. The signal is observed for different probe beam diameter of 0.25 mm, 0.87 mm, 1.57 mm, 2.30 mm.

The probe region is kept close to the nozzle and expected bubble size is $\approx$ 1 mm. The obtained result is shown is figure 5.9 (a). By increasing the size of the beam diameter the fall and rise of PBD signal becomes more gradual in nature. By fitting the segment from zero level to the negative peak linearly it is found that the slope increases from 2.83 to 62.31. The slope for different beam diameter is tabulated in Table 1 in inset of Fig. 5.9 (b). The time constant derived by exponentially fitting the growth from negative to zero level also increases from 0.02163 s to 0.06825 s with beam diameter. The time constant value obtained for different beam diameter is tabulated in Table 2 in inset of Fig. 5.9 (c). The reason for observed signal is classified and

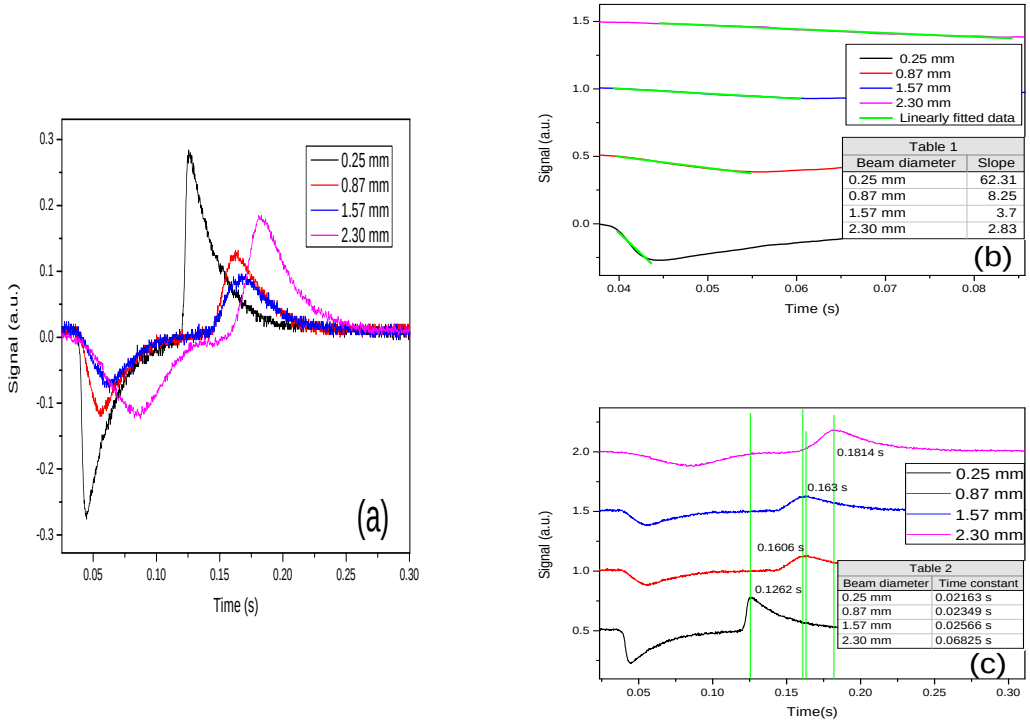

Figure 5.9: PBD signal of air bubble moving in glycerine as liquid medium recorded for different probe beam diameter (a), linear fitted signal segment (b), shift of positive peak in time (c). In inset of (b) and (c) tabel is displayed showing the obtained slope and time constant respectively.

explained in two parts (i) beam size < bubble size (ii) beam size > bubble size.

Case 1: Beam Size < Bubble Size: For beam size less than bubble size as shown in Fig. 5.10 the beam can be approximated as ray. Hence rise and fall of the signal would be sharp as seen in Fig. 5.9 (a) for beam size of 0.25 mm. Since beam size is small bubble pass the beam immediately. Hence the time constant of exponential growth would be less.

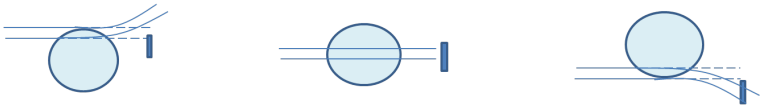

Figure 5.10: Beam deflection phenomenon when laser beam diameter is less than bubble diameter.

Case 2: Beam Size > Bubble Size: For beam size greater than bubble size as shown in Fig. 5.11 the beam will be cover most of the bubble

surface and hence exponential part of the equation 5.10 will always be present. Hence the gradual increase and decrease in signal will be obtained as indicated by the increase in the slope with increase in beam diameter (see Table 2 in inset of Fig. 5.9 (c)). The time constant of exponential growth will be more as bubble spend more time in the beam. Beacause of bubble spending more time in the beam the appearence of positive peak will shift towards right as shown in Fig. 5.9 (c). Hence the gradual increase and decrease of signal is obtained.

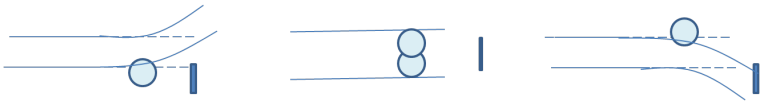

Figure 5.11: Beam deflection phenomenon when laser beam diameter is greater than bubble diameter.

5.3.3 Effect of Change in Probe Region

In this section, the air bubble is probed at different height measured from the nozzle. For this measurement beam diameter was kept constant. The result obtained is shown is Fig. 5.12.

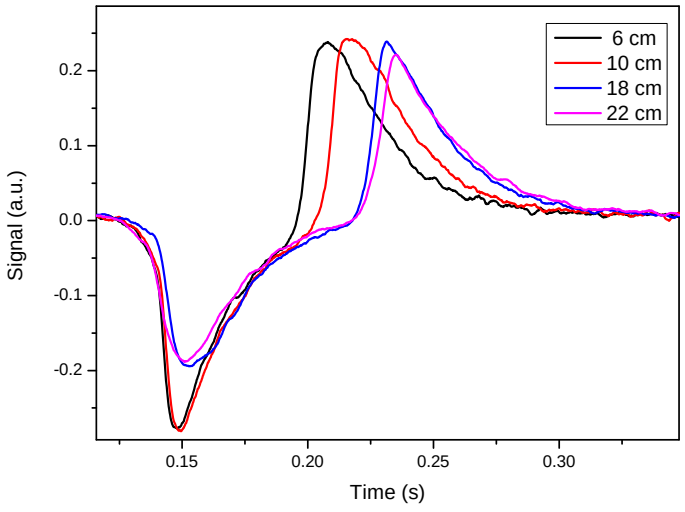

Figure 5.12: Probe beam deflection signal for different probe region above the nozzle. The black, red, blue, violet curve represents signal for probe beam positioned at 6 cm, 10 cm, 18 cm, 22 cm above the nozzle respectively.

By exponential fitting the growth of signal from negative to zero level no significant difference is observed. As per Stokes's law velocity

should increase as the bubble rises in column. Hence we expected that with change in height signals would change from symetric to asymmetric nature. Absence of this in our signal indicates that range in which height is been changed, no significant change in velocity can be attained. As in the previous measurement (see Fig. 5.9(c)) the shift of positive peak can be observed. The shift can be attributed to the shape deformation of bubble from shperical to elliptical. By attaining the elliptical shape the bubble size becomes smaller in perpendicular direction with reference to the beam size.

Chapter 6

Conclusion and Future Prospects

6.1 Conclusion:

In this work we have studied the qualitative and quantitatve difference between the following the five model (a) Rayleigh-Plesset's model. (b) Herring's model. (c) Flynn's model. (d) Keller-Miksis's model. (e) Gilmore's model. By simulation work we concluded the followings

1. Numerical simulation of a any particular cavitation bubble dynamics model shows the bubble radius oscillates about an equllibrium radius value.
2. All compressible bubble dynamics models gives almost same value of maximum bubble radius for the first oscillation.
3. Compressible bubble models shows significant damping in bubble radius oscillation than in-compressible one.
4. The parameter optimization gives us an idea about how bubble dynamics changes with the change in liquid properties such as viscosity, surface tension, density etc.
5. Again simulation work tells us about the maximum bubble radius attained by the bubble for fixed ambient pressure, liquid properties.

At the end of the work we have developed the beam deflection technique to detect the moving air bubble in liquid medium and following observations are made.

1. Air bubble while moving through liquid medium will have bipolar type response.

2. For viscous liquid the signal will be more symmetric as compared to less viscous.

3. By increasing the beam diameter in compare to bubble size the signal can be made symmetric.

4. Contrary to Stokes's law on significant change in the velocity is been observed for the given height of our liquid column.

6.2 Future Prospects:

Proposed Simulation work: Nowadays cavitation bubble generation, by pulsed laser, in liquid media is a popular method particularly due to it's wide applicability in Medical Science and Technology. Very few theoretical works, related to the simulation of cavitation bubble dynamics in presence of a pulsed laser, are reported. In view of the current scenario of this field we propose the following theoretical work:

1. Simulation of cavitation bubble dynamics in presence of a pulsed laser field and to study the effects of laser parameters like pulse duration, laser power, beam profile, wavelength, frequency etc on the bubble dynamics.

2. Also to study the effect of temperature on cavitation bubble dynamics.

Proposed Experiment: In our experimental observation we have been able to understand the air bubble-laser interaction phenomenon. The simulation part gives quantitative idea about bubble parameters like radius, oscillation time etc. In order to verify the simulated result by our probe beam deflection technique the stable isolated bubble would be required. Laser induced cavitation bubble is one which generates due to the cavity formation caused dielectric breakdown hence plasma formation as well as it's expansion. As the time passes due to heat diffusion, mass diffusion cavity disappears within micro scale of time [13, 12]. It wolud be interesting to develop PBD technique to probe this bubbles. Altough other vaious techniques like high speed photography, ultra sound pizo-electric transducer etc exsits[12]. A high speed photography technique can be use as a comparative method of

PBD. A schematic diagram of laser induced cavitation bubble detection by probe beam deflection technique has been shown in figure 6.1. A pulsed laser can be used as pump to generate transient bubble in

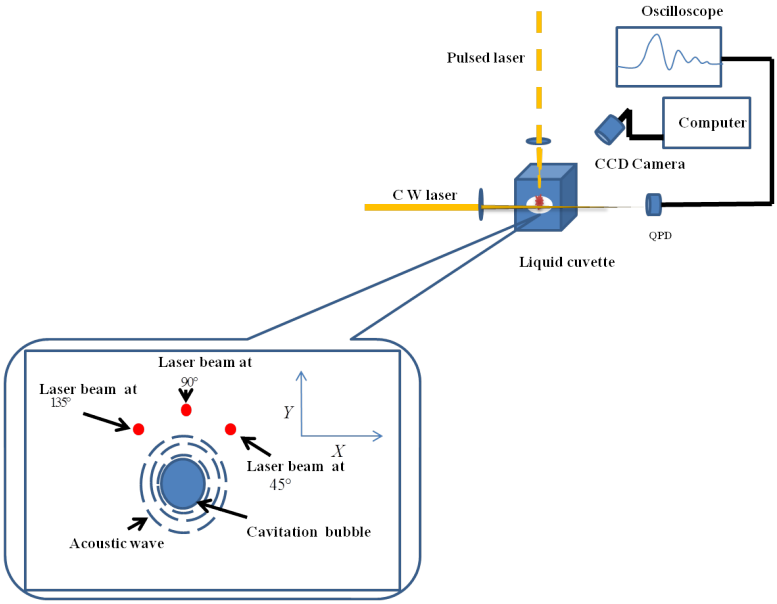

Figure 6.1: Diagram of proposed experimental setup.

a liquid medium. A CW laser at perpendicular to the pump will act as probe beam. The probe beam deflection due to cavitation bubble dynamics can be trace with the help of a QPD. A high speed camera placed perpendicular to both pump and probe will capture the cavitation bubble evolution moments.

Bibliography

[1] Lord Rayleigh. Viii. on the pressure developed in a liquid during the collapse of a spherical cavity. *The London, Edinburgh, and Dublin Philosophical Magazine and Journal of Science*, 34(200):94–98, 1917.

[2] Conyers Herring. *Theory of the pulsations of the gas bubble produced by an underwater explosion.* Columbia Univ., Division of National Defense Research, 1941.

[3] Leon Trilling. The collapse and rebound of a gas bubble. *Journal of Applied Physics*, 23(1):14–17, 1952.

[4] Forrest R Gilmore. The growth or collapse of a spherical bubble in a viscous compressible liquid. 1952.

[5] John G Kirkwood. *Progress Report on" The Pressure Wave Produced by an Underwater Explosion III" to August 15, 1942.* National Defense Research Committee of the Office of Scientific Research and Development, 1942.

[6] Hugh G Flynn. Cavitation dynamics. i. a mathematical formulation. *The Journal of the Acoustical Society of America*, 57(6):1379–1396, 1975.

[7] Joseph B Keller and Ignace I Kolodner. Damping of underwater explosion bubble oscillations. *Journal of applied physics*, 27(10):1152–1161, 1956.

[8] Shigeo Fujikawa and Teruaki Akamatsu. Effects of the non-equilibrium condensation of vapour on the pressure wave produced by the collapse of a bubble in a liquid. *Journal of Fluid Mechanics*, 97(3):481–512, 1980.

[9] Telli Faez, Marcia Emmer, Klazina Kooiman, Michel Versluis, Antonius FW van der Steen, and Nico de Jong. 20 years of ultra-

sound contrast agent modeling. *IEEE transactions on ultrasonics, ferroelectrics, and frequency control*, 60(1), 2013.

[10] Nico de Jong and L Hoff. Ultrasound scattering properties of albunex microspheres. *Ultrasonics*, 31(3):175–181, 1993.

[11] Philippe Marmottant, Sander van der Meer, Marcia Emmer, Michel Versluis, Nico de Jong, Sascha Hilgenfeldt, and Detlef Lohse. A model for large amplitude oscillations of coated bubbles accounting for buckling and rupture. *The Journal of the Acoustical Society of America*, 118(6):3499–3505, 2005.

[12] Paul K Kennedy, Daniel X Hammer, and Benjamin A Rockwell. Laser-induced breakdown in aqueous media. *Progress in quantum electronics*, 21(3):155–248, 1997.

[13] Alfred Vogel, S Busch, and U Parlitz. Shock wave emission and cavitation bubble generation by picosecond and nanosecond optical breakdown in water. *The Journal of the Acoustical Society of America*, 100(1):148–165, 1996.

[14] Alfred Vogel, Stefan Busch, Kerstin Jungnickel, and Reginald Birngruber. Mechanisms of intraocular photodisruption with picosecond and nanosecond laser pulses. *Lasers in surgery and medicine*, 15(1):32–43, 1994.

[15] B Zysset, JG Fujimoto, and TF Deutsch. Time-resolved measurements of picosecond optical breakdown. *Applied Physics B: Lasers and Optics*, 48(2):139–147, 1989.

[16] H Schmidt-Kloiber, G Paltauf, and E Reichel. Investigation of the probabilistic behavior of laser-induced breakdown in pure water and in aqueous solutions of different concentrations. *Journal of applied physics*, 66(9):4149–4153, 1989.

[17] Alfred Vogel, Ingo Apitz, Sebastian Freidank, and Rory Dijkink. Sensitive high-resolution white-light schlieren technique with a large dynamic range for the investigation of ablation dynamics. *Optics letters*, 31(12):1812–1814, 2006.

[18] A Vogel, W Lauterborn, and R Timm. Optical and acoustic investigations of the dynamics of laser-produced cavitation bubbles near a solid boundary. *Journal of Fluid Mechanics*, 206:299–338, 1989.

[19] B Ward and DC Emmony. Interferometric studies of the pressures developed in a liquid during infrared-laser-induced cavitation-bubble oscillation. *Infrared physics*, 32:489–515, 1991.

[20] CE Bell and JA Landt. Laser-induced high-pressure shock waves in water. *Applied Physics Letters*, 10(2):46–48, 1967.

[21] Amol A Kulkarni and Jyeshtharaj B Joshi. Bubble formation and bubble rise velocity in gas- liquid systems: a review. *Industrial & Engineering Chemistry Research*, 44(16):5873–5931, 2005.

[22] AK Khurana and Rajinder Kumar. Studies in bubble formation?iii. *Chemical Engineering Science*, 24(11):1711–1723, 1969.

[23] Robert J Benzing and John E Myers. Low frequency bubble formation at horizontal circular orifices. *Industrial & Engineering Chemistry*, 47(10):2087–2090, 1955.

[24] R Kumar and NK Kuloor. The formation of bubbles and drops. *Advances in chemical engineering*, 8:255–368, 1970.

[25] AS Vasilev. Laws governing the outflow of a jet of gas into a liquid. *Theor. Found. Chem. Eng*, 4(5):727, 1970.

[26] HIDEKI TSUGE and SHIN-ICHI HIBINO. Bubble formation from an orifice submerged in liquids. *Chemical Engineering Communications*, 22(1-2):63–79, 1983.

[27] RM Davies and Geoffrey Taylor. The mechanics of large bubbles rising through extended liquids and through liquids in tubes. In *Proceedings of the Royal Society of London A: Mathematical, Physical and Engineering Sciences*, volume 200, pages 375–390. The Royal Society, 1950.

[28] Jerry Namery. Ultrasonic bubble detector, August 17 1976. US Patent 3,974,681.

[29] Rok Petkovšek and Peter Gregorčič. A laser probe measurement of cavitation bubble dynamics improved by shock wave detection and compared to shadow photography. *Journal of Applied Physics*, 102(4):044909, 2007.

[30] Peter Gregorčič, Rok Petkovšek, and Janez Možina. Investigation of a cavitation bubble between a rigid boundary and a free surface. *Journal of applied physics*, 102(9):094904, 2007.

[31] WP Schiffers, SJ Shaw, YH Jin, and David C Emmony. High-speed photographic study of the interaction of cavitation bubbles with a boundary. In *22nd International Congress on High-Speed Photography and Photonics*, volume 2869, pages 308–316. International Society for Optics and Photonics, 1997.

[32] James E Chomas, Paul A Dayton, Donovan May, John Allen, Alexander Klibanov, and Katherine Ferrara. Optical observation of contrast agent destruction. *Applied Physics Letters*, 77(7):1056–1058, 2000.

[33] Karen E Morgan, John S Allen, Paul A Dayton, James E Chomas, AL Klibaov, and Katherine W Ferrara. Experimental and theoretical evaluation of microbubble behavior: Effect of transmitted phase and bubble size. *IEEE transactions on ultrasonics, ferroelectrics, and frequency control*, 47(6):1494–1509, 2000.

[34] R Pecha, B Gompf, G Nick, ZQ Wang, and W Eisenmenger. Resolving the sonoluminescence pulse shape with a streak camera. *Physical review letters*, 81(3):717, 1998.

[35] GP Davidson and DC Emmony. A schlieren probe method for the measurement of the refractive index profile of a shock wave in a fluid. *Journal of Physics E: Scientific Instruments*, 13(1):92, 1980.

[36] G Koren. Observation of shock waves and cooling waves in the laser ablation of kapton films in air. *Applied physics letters*, 51(8):569–571, 1987.

[37] Janez Diaci. Response functions of the laser beam deflection probe for detection of spherical acoustic waves. *Review of scientific instruments*, 63(11):5306–5310, 1992.

[38] Jeffrey A Sell, David M Heffelfinger, Peter Ventzek, and Ronald M Gilgenbach. Laser beam deflection as a probe of laser ablation of materials. *Applied Physics Letters*, 55(23):2435–2437, 1989.

[39] Hongping Guo and Qihong Lou. The study of the processes of laser-induced vaporization of copper surface by time-resolved laser beam deflection technique. *Optics communications*, 77(5-6):381–384, 1990.

[40] B Sullivan and AC Tam. Profile of laser-produced acoustic pulse in a liquid. *The Journal of the Acoustical Society of America*, 75(2):437–441, 1984.

[41] Andrew C Tam. Applications of photoacoustic sensing techniques. *Reviews of Modern Physics*, 58(2):381, 1986.

[42] Markus W Sigrist. Laser generation of acoustic waves in liquids and gases. *Journal of applied physics*, 60(7):R83–R122, 1986.

[43] Alan J Walton and Geo T Reynolds. Sonoluminescence. *Advances in Physics*, 33(6):595–660, 1984.

[44] cf eg PS Epstein and Milton S Plesset. On the stability of gas bubbles in liquid-gas solutions. *The Journal of Chemical Physics*, 18(11):1505–1509, 1950.

[45] F Ronald Young. *Cavitation*. World Scientific, 1999.

[46] Christopher E Brennen. *Cavitation and bubble dynamics*. Cambridge University Press, 2013.

[47] VP Skripov. 1974, metastable liquids, john wiley & sons, new york.

[48] GA Khoroshev. Collapse of vapor-air cavitation bubbles(collapse of single spherical vapor-air cavitation bubble, computing bubble movement and pressure as function of air content). *Soviet Physics-Acoustics*, 9:275–279, 1964.

[49] H Poritsky. The growth or collapse of a spherical bubble or cavity in a viscous fluid. In *Proc. US First National Congress, Appl. Mech., ASME*, volume 313, 1952.

[50] Robert H Cole and Royal Weller. Underwater explosions. *Physics Today*, 1:35, 1948.

[51] Robert T Knapp, James W Daily, and Frederick G Hammitt. *Cavitation*. McGraw-Hill, 1970.

[52] A Mallock. The damping of sound by frothy liquids. *Proceedings of the Royal Society of London. Series A, Containing Papers of a Mathematical and Physical Character*, 84(572):391–395, 1910.

[53] GJ Lastman and RA Wentzell. Comparison of five models of spherical bubble response in an inviscid compressible liquid. *The Journal of the Acoustical Society of America*, 69(3):638–642, 1981.

[54] K Vokurka. A method for evaluating experimental data in bubble dynamics studies. *Czechoslovak journal of physics*, 36(5):600–615, 1986.

[55] D Papoulias and M Gavaises. Modelling of single bubble-dynamics and thermal effects. In *Journal of Physics: Conference Series*, volume 656, page 012098. IOP Publishing, 2015.

[56] Detlef Lohse and Sascha Hilgenfeldt. Inert gas accumulation in sonoluminescing bubbles. *The Journal of chemical physics*, 107(17):6986–6997, 1997.

[57] Guilherme Dutra, Cicero Martelli, Marco José Da Silva, Rodolfo L Patyk, and Rigoberto EM Morales. Air flow detection in crude oil by infrared light. *Sensors*, 17(6):1278, 2017.

[58] DF Swinehart. The beer-lambert law. *Journal of chemical education*, 39(7):333, 1962.

[59] Ronald A Barnes Jr. Implementing the probe beam deflection technique for acoustic sensing in photoacoustic and ultrasound imaging.

[60] Václav Tesař. Microbubble generation by fluidics, part ii: Bubble formation mechanism. In *Proc. of Colloquium Fluid Dynamics*, 2012.

[61] Václav Tesař and Miroslav Jílek. Integral fluidic generator of microbubbles.

[62] Wim Van Hoeve, Benjamin Dollet, Michel Versluis, and Detlef Lohse. Microbubble formation and pinch-off scaling exponent in flow-focusing devices. *Physics of fluids*, 23(9):092001, 2011.

[63] Yutao Lu, Taotao Fu, Chunying Zhu, Youguang Ma, and Huai Z Li. Pinch-off mechanism for taylor bubble formation in a microfluidic flow-focusing device. *Microfluidics and nanofluidics*, 16(6):1047–1055, 2014.

[64] R Bolanos-Jiménez, A Sevilla, C Martinez-Bazan, D Van Der Meer, and JM Gordillo. The effect of liquid viscosity on bubble pinch-off. *Physics of fluids*, 21(7):072103, 2009.